CHALMERS

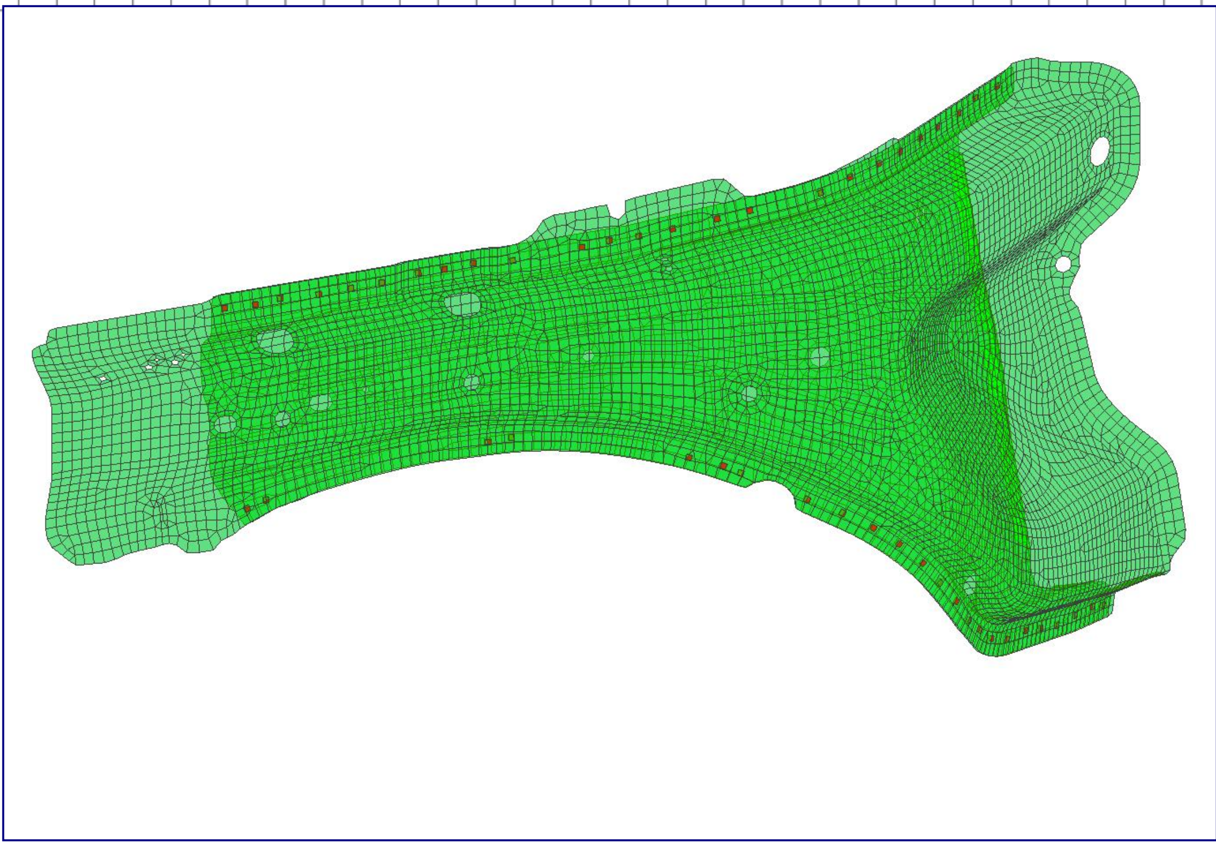

Modelling of spot welds for NVH simulations in view of refined panel meshes

Master's Thesis in the Master's programme in Sound and Vibration

TORSTEN EPPLER & ROLF SCHATZ

Department of Civil and Environmental Engineering
Division of Applied Acoustics
Chalmers Vibroacoustics Group
CHALMERS UNIVERSITY OF TECHNOLOGY
Göteborg, Sweden 2007

Master's Thesis 2007:150

MASTER'S THESIS 2007:150

Modelling of spot welds for NVH simulations in view of refined panel meshes

TORSTEN EPPLER & ROLF SCHATZ

Department of Civil and Environmental Engineering
Division of Applied Acoustics
Vibroacoustics Group
CHALMERS UNIVERSITY OF TECHNOLOGY
Göteborg, Sweden 2007

Modelling of spot welds for NVH simulations in view of refined panel meshes

Master's Thesis 2007:150

Department of Civil and Environmental Engineering
Division of Applied Acoustics
Vibroacoustics Group
Chalmers University of Technology
SE-41296 Göteborg
Sweden

Tel. +46-(0)31 772 1000

Reproservice / Department of Civil and Environmental Engineering
Göteborg, Sweden 2007

Modelling of spot welds for NVH simulations in view of refined panel meshes
Master's Thesis in the Master's programme in Sound and Vibration
TORSTEN EPPLER & ROLF SCHATZ
Department of Civil and Environmental Engineering
Division of Applied Acoustics
Vibroacoustics Group
Chalmers University of Technology

Abstract

Today spot welding is the most common technique for connecting metal parts of an automotive body. A few thousands of these spot welds are applied to a car body in-white during an automated assembly process. Therefore it's obvious that the dynamic behaviour of an automotive body is highly affected by these connections. In the Computer-Aided Engineering (CAE) processes exist different Finite Element (FE) modelling approaches for spot weld connections, depending on the area of interest like Noise-Vibration-Harshness (NVH), durability etc. For NVH simulations ACM2 and CWELD spot weld approach are mostly used in industry.
The aim of the present work is to investigate these most common spot weld models for NVH in view of a refined FE-mesh. In addition to the refined meshes the influence of a detailed thickness distribution over the metal sheets is studied. If necessary, an updating process should be elaborated for the most suitable spot weld model, so that it can be used with refined meshes. For validation purpose eigenfrequencies and frequency response functions (FRF's) from FE-simulation and measurements will be compared.

Keywords: Finite Element analysis, Structural dynamics, Spot weld, ACM2, CWELD, mesh refinement, NVH

Contents

Acknowledgements

First of all we want to thank the Department of Applied Acoustics for offering us the possibility and providing us with all the needed support for conducting this thesis work.
Our special thank is dedicated to Professor Wolfgang Kropp and Andrzej Pietrzyk, which supervised our work and gave helpful advices in many discussions. But also all the other members of the department have to be mentioned, giving us help and having an open ear during the whole time.
Also special thanks to Börje Wijk who spent a lot of time helping us all with the measurement equipment and especially in building up a workstation.
Finally a big thank you to our Swedish landlord Kent Holzner and his whole family for doing us our stay in Sweden as pleasantly as possible including the numerous unforgetable sailing trips and dinners.

1 Introduction

Spot weld modeling is the main joining technique for car body panels. For a typical car body one can assume several thousands of spot welds. The joining process itself happens with two electrodes applying pressure to the metal sheets when welding them together. The spot weld itself results from metal fusion. During that process the spot weld nugget gets a different material property like the original metal sheets and also a zone around the nugget is affected from the produced heat which affects as well the material properties.

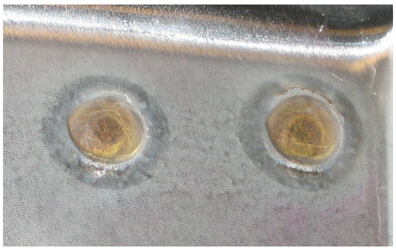

For FEM simulation it is difficult to describe boundary conditions of those spot weld positions precisely. From the point of view of NVH calculations it is obviously that these joints mainly influence the stiffness behavior of the whole structure. Therefore several spot weld models have been created in the past. The most widely used spot weld models in industry are the CWELD model and the ACM2 model. The standard model at Volvo is the ACM2 model, because it has like the CWELD model the important benefit to be able to connect independently meshed structures together.

With increasing calculation power there is also a demand to refine the mesh size with the aim to get more accurate simulation results at higher frequencies. The reason therefore is, that components of a car body mainly consists of complex structures. Another important fact is, that the choice of finite element formulation is always a compromise between the demands of NVH-, Crash-, and Durability simulations. Also very small holes and bolts can only be modeled exactly with small enough mesh sizes. On the other hand with further mesh refinement the position of spot welds and also their dynamic properties should not be affected. Previous investigations at Volvo show that the current modeling technique (ACM2) shows weakness with further refinement of the body panel meshes.

1.1 Aim of this thesis

The aim of this thesis can be split up in following parts:

Preliminry part

1. Literature study regarding spot weld modeling in vehicle bodies.
2. Getting acquainted with *MSC Nastran* analysis procedures relevant for dynamic analysis and development of a Postprocessing Toolbox in *Matlab*

Main part

1. Carrying out FRF tests on two sets of benchmark structures (inner and outer panel) in free-free conditions
2. Carrying out simulations of the above experiments, including metal forming data and different mesh densities
3. Carrying out FRF measurements on the welded benchmark structures
4. Carrying out simulations of the welded benchmark structure, using different spot weld models and mesh densities, including metal forming
5. Comparison of test results and simulation results
6. Selection of the most interesting candidates for future applications

1.2 Post processing Toolbox in Matlab

The FEM calculations in this thesis were done with *MD Nastran*. *Nastran* itself is only the solver which means that to carry out a whole analysis one has to work also with some kind of Pre- and Postprocessor. The preprocessing process encircles the construction of an FEM model with the help of available CAD data. The whole model was stored in a separate mesh-data-file. The analysis setup was stored in a separate analysis-file. The construction of all desired FEM models was done at Volvo. The calculation of the models was done at Chalmers. To visualize the analysis results in some way it was necessary to load the numerical calculation results in *Matlab*. Therefore a postprocessing Toolbox has been developed.

The postprocessing Toolbox consists of following programmes:

- *nas2mat.m* : function which reads the whole mesh-file and stores it in a workspace.
- *read_eigenvector.m* : function which reads the eigenvectors of all nodes from the Punch-file for each corresponding eigenfrequency and stores the eigenvectors in a workspace
- *read_FRF.m* : function which reads the calculated displacement data from the Punch-files.
- *calculate_frf.m* : function which calculates all FRFs from the displacement results
- *plot_geometry.m* : function which plots the whole mesh-data
- *animate_mode.m* : function which animates the calculated modes of the structure
- *plot_mode.m* : function which plots pictures from the mode shapes

2 Theoretical Background

In this chapter a short overview will be given about spot weld models which are present in literature. The focus is set on models which are normally used in the area of Noise-Vibration-Harshness (NVH) simulations.

2.1 CWELD

The CWELD approach was introduced in *MSC.Nastran* 2001 [09, 19]. Further element descriptions and verification investigations can be found in [02, 04]. The CWELD element full fills the main requirements that it can connect non congruent meshes as well as congruent and the weld area is considered.
With the CWELD element three types of connections can be defined:

- A Point to Point connection, where an upper and lower shell grid are connected
- A Point to Patch connection; where a grid point of a shell is connected to a surface patch
- A Patch to Patch connection, where a spot weld grid GS is connected to an upper and lower surface patch (see figure 2.1)

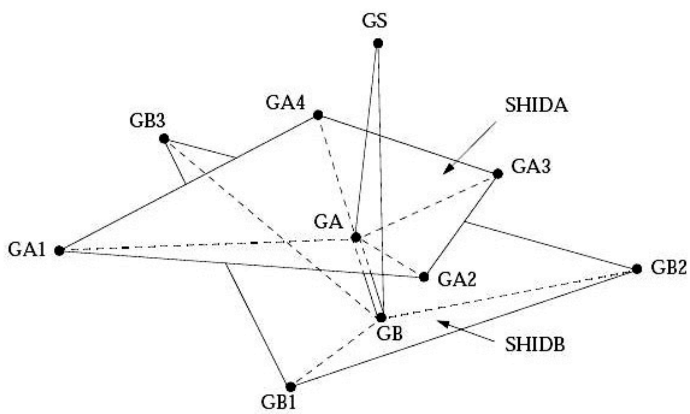

Figure 2.1: CWELD spot weld with Patch to Patch connection [09]

The Patch to Patch connection is the most general connectivity and is considered here in the following explanations. The center of the weld is defined by the spot weld grid GS, which is usually not a node in the FE-mesh and it isn't required that GS lies on the FE-geometry. The CWELD algorithm projects GS normal to the upper shell and the resulting piercing point is called GA. The direction GS-GA defines the piercing point GB on the lower shell. The projected grids GA and GB define the length and direction of the spot weld itself.
CWELD allows connections up to 10 layers and works with different element types. For example quadrilateral and triangular elements can be connected. A surface patch must have at least 3 grids and has an upper limit of 8 grids.
The spot weld itself is a short beam between GA and GB with 2x6 degrees of freedom (see figure 2.2). The element is a special shear flexible beam of the type Timoshenko. The Young's modulus and spot weld diameter D are taken from the material defined on the PWELD property entry. The cross sectional properties like the shear modulus are calculated with the spot diameter D. The length of the beam is the distance between GA and GB.

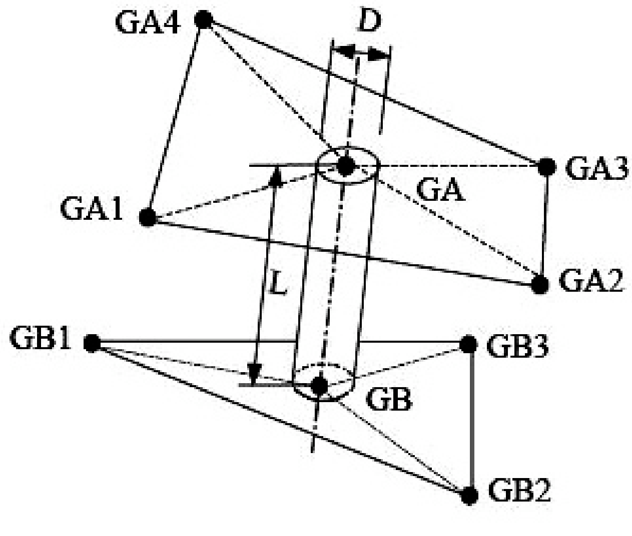

Figure 2.2: Spot weld element [19]

If on the PWELD property SPOT is defined, an effective element length L_e is defined, regardless of the true length like:

$$L_e = \frac{1}{2} \cdot (t_a + t_B) \tag{2.1}$$

t_a and t_B are the thickness of the involved plates (shells)

Then the Young's and shear modulus E and G are scaled by the ratio of true length to the effective length:

$$\widetilde{E} = E \cdot \frac{L}{L_e} \quad \widetilde{G} = G \cdot \frac{L}{L_e} \tag{2.2}$$

This scaling leads to a spot weld stiffness which is approximately constant for all elements. Additionally extremely elements with short lengths L and extremely soft elements with long lengths L are avoided. If SPOT is not defined the true length is used if it is inside the range:

$$LDMIN \leq L/D \leq LDMAX \tag{2.3}$$

LDMIN and LDMAX could be defined by the user and are by default: LDMIN = 0.2 and LDMAX = 5.0
For the patch to patch connection the beam end points GA and GB are connected to the shell grids of shell A and B with the help of constraint equations. The underlying method is subsequently described and the equations are shown exemplary for grid point A. The three translational DOF of grid GA are connected with the three translational DOF of the shell grid points using the interpolation functions of the corresponding shell surface. The three rotational DOF at grid GA are connected to the three translational DOF of the shell grid points with Kirchhoff conditions.

$$\begin{Bmatrix} u \\ v \\ w \end{Bmatrix}_A = \sum N_I \left(\xi_A, \eta_A\right) \cdot \begin{Bmatrix} u \\ v \\ w \end{Bmatrix}_I \tag{2.4}$$

$$\begin{aligned} \theta_x^A &= \frac{\partial w}{\partial y} = \sum N_{I,y} \cdot w_I \\ \theta_y^A &= -\frac{\partial w}{\partial x} = -\sum N_{I,x} \cdot w_I \\ \theta_z^A &= \frac{1}{2}\left(\frac{\partial v}{\partial x} - \frac{\partial u}{\partial y}\right) = \frac{1}{2}\left(\sum N_{I,x} \cdot v_I - \sum N_{I,y} \cdot u_I\right) \end{aligned} \tag{2.5}$$

N_I : shape functions of the surface patch
ξ_A and η_A : normalized coordiantes of GA
u, v, w : displacements
$\theta_x, \theta_y, \theta_z$: rotations

These 6 equations are written in the local tangent system of the surface patch at point GA. The normal direction is z and the tangent directions are x and y. The patch to patch connection ends up with 12 constraint equations.
For the formats GRIDID and ELEMID, the grid points are corresponding with grid points of shell elements. For the new formats ELPAT and PARTPAT, the grid points are auxiliary points GAHI and GBHI, I=1,4, constructed like shown in figure (2.3).

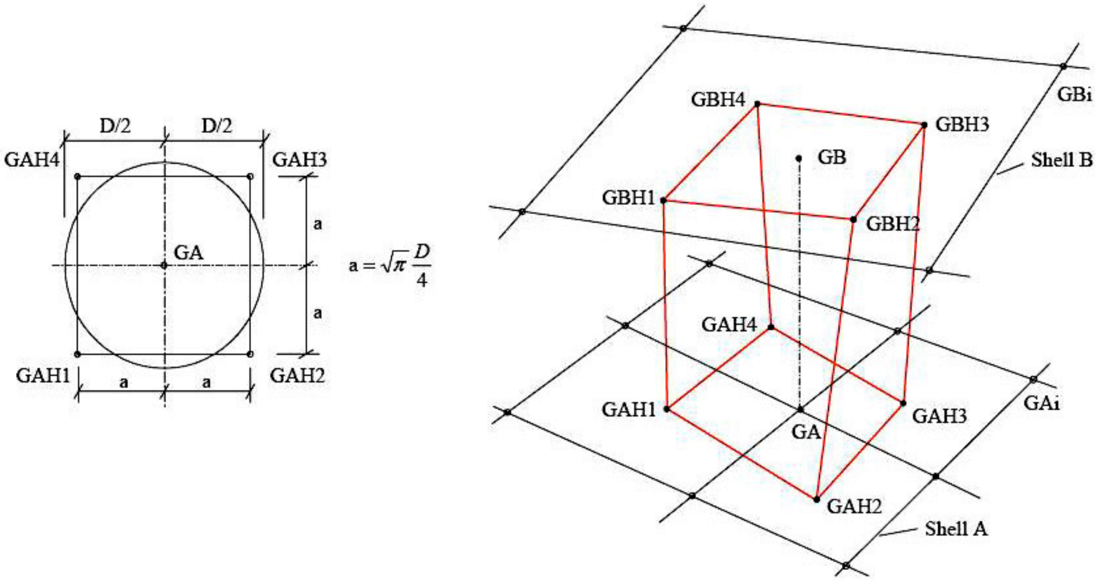

Figure 2.3: Cross sectional area and auxiliary points GAHI and GBHI for formats ELPAT and PARTPAT [19]

The auxiliary points are connected to shell element grids with a second set of following constraints:

$$\begin{Bmatrix} u \\ v \\ w \end{Bmatrix}_I = \sum_K G_{IK} \cdot \begin{Bmatrix} u \\ v \\ w \end{Bmatrix}_K \tag{2.6}$$

G_{IK} : coefficient matrix derived from RBE3 type constraints
K : shell grid points

With the formats ELPAT and PARTPAT, the CWELD element can connect from one up to 3x3 elements on shell A resp B, which is presented in figure (2.4)

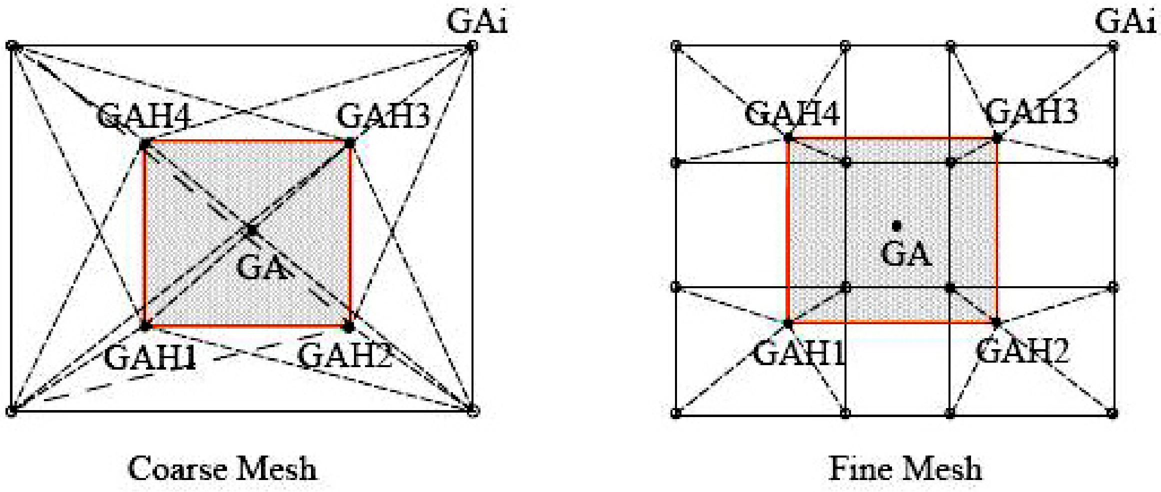

Figure 2.4: Connectivity for formats ELPAT and PARTPAT [19]

Studies in [2] show that the CWELD approach simulates the force transfer between a patch to patch connection accurately for

$$D/S \leq 1.0 \tag{2.7}$$

D : spot diameter
S : mesh size (length of shell element)

2.2 ACM2 model

In [03] the ACM2 model was proposed. Figure (2.5) shows a typical construction of the model. The ACM2 model consists of a brick element which is coupled at the corners to the upper and the lower shell elements over RBE3 elements. All connected shell elements build up a so-called patch area. The RBE3 elements are interpolation elements which make it possible to connect two non-congruent meshes without the need to remesh around the coupling zones.

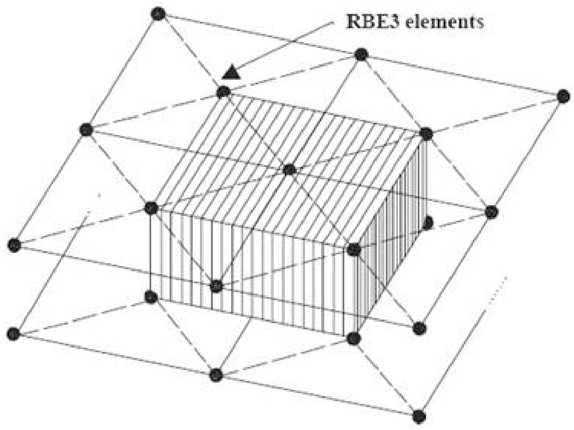

Figure 2.5: A typical construction of an ACM2 model from [01]

The RBE3 element itself can lie inside a shell element and its displacement corresponds to the weighted average of the displacements of the surrounding grid points. In the ACM2 formulation the weighting factors of the RBE3 connection nodes depend on the shape displacement functions for the underlying shell element. If the underlying element formulation corresponds to a quadrilateral shell element like drawn in figure (2.6), the displacement u_P of any point inside the surface can be written like in equation (2.8).

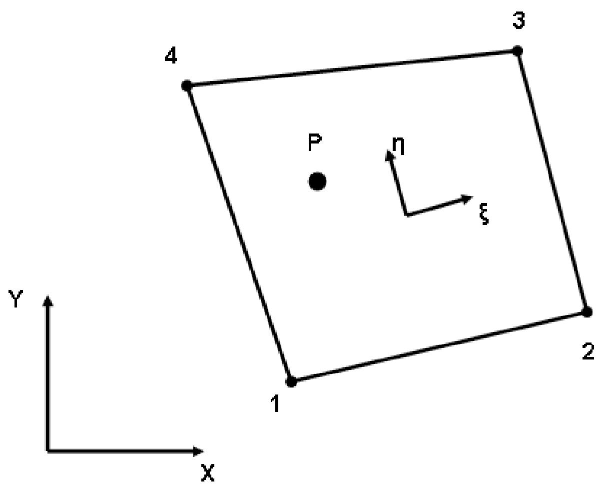

Figure 2.6: The displacement in isoparametric formulation

$$u_P = W_1 u_1 + W_2 u_2 + W_3 u_3 + W_4 u_4 \tag{2.8}$$

W_i are exactly the desired weighting factors needed for the RBE3 input. The sum over all weighting functions is 1.

$$\sum_{i=1}^{n} W_i = 1 \tag{2.9}$$

The weighting functions depends on the isoparametric coordinates ξ and η. These coordinates have the value 1 or -1 at the corner grid points. The weighting for each corner grid point is calculated as follows:

$$\begin{aligned}
W_1 &= \frac{1}{4}\left(1-\xi\right)\left(1-\eta\right) \\
W_2 &= \frac{1}{4}\left(1+\xi\right)\left(1-\eta\right) \\
W_3 &= \frac{1}{4}\left(1+\xi\right)\left(1+\eta\right) \\
W_4 &= \frac{1}{4}\left(1-\xi\right)\left(1+\eta\right)
\end{aligned} \tag{2.10}$$

If for example point P concur with one of the corner grid points, the corresponding weighting factor will be 1 and the other factors will be zero. In general for the locations of the RBE3 elements ξ and η are unknown. In [11] the mathematical procedure is described in detail. The starting point for an quatrilateral shell element are 4 unknown weighting factors. Therefore four independent equations as follows are needed.

$$\begin{aligned}
x_P &= W_1 u_{x1} + W_2 u_{x_2} + W_3 u_{x_3} + W_4 u_{x_4} \\
x_P &= W_1 u_{y1} + W_2 u_{y_2} + W_3 u_{y_3} + W_4 u_{y_4} \\
1 &= W_1 + W_2 + W_3 + W_4 \\
0 &= W_1 \cdot W_2 - W_3 \cdot W_4
\end{aligned} \tag{2.11}$$

In equation (2.11) one can see that the equation system becomes nonlinear because it includes a product of variables. There exsists many iterative solution methods, to solve such eqations systems. An illustrative description of the Newton-Raphson method is given in [11].

The area of the brick element corresponds like for the CWELD model to the equivalent cross section area of the real spot weld. Figure (2.7) illustrates, how the size a of the brick element is related to the real spot weld.

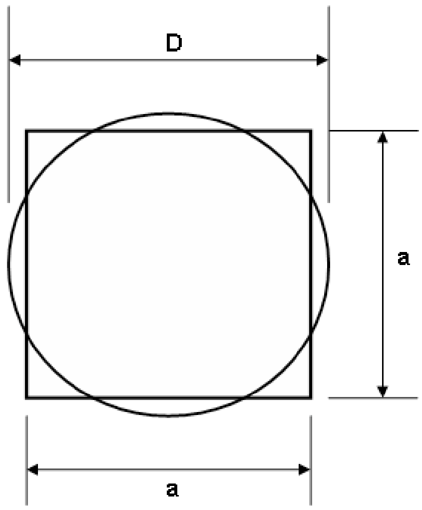

Figure 2.7: The equivalet cross section area of the brick element

With the given diameter D of the real spot welds on the structure the size a of the hexa element will be calculated with following equation

$$a = \sqrt{\frac{\pi d^2}{4}} \tag{2.12}$$

In Pre-processors like *ANSA* there is a possibility to enlarge the size of a brick element with the help of a so-called area factor (af). This factor enlarges the area of a hexa element with a factor multiplied to the origin area. If for example the area factor has the value 3, the size of the brick element corresponds to that length needed to increase the cross section area of the hexa element 3 times the origin one.

An important fact is that the weighting procedure depending on the linear shape function ensures that the center of highest stiffness is always in the center of the brick element regardless of its location in the mesh. Due to the fact that the center node is connected with all 4 corner nodes of the brick element it acquires the strongest coupling with the brick element. The weighting factor depending on the shape function of all the connected shell elements constructs a "stiffness near field"which radiates on the coupled patch area like drawn in figure (2.8). So we can assume the near field around the spot weld as a monopol with an equal stiffness distribution in all directions.

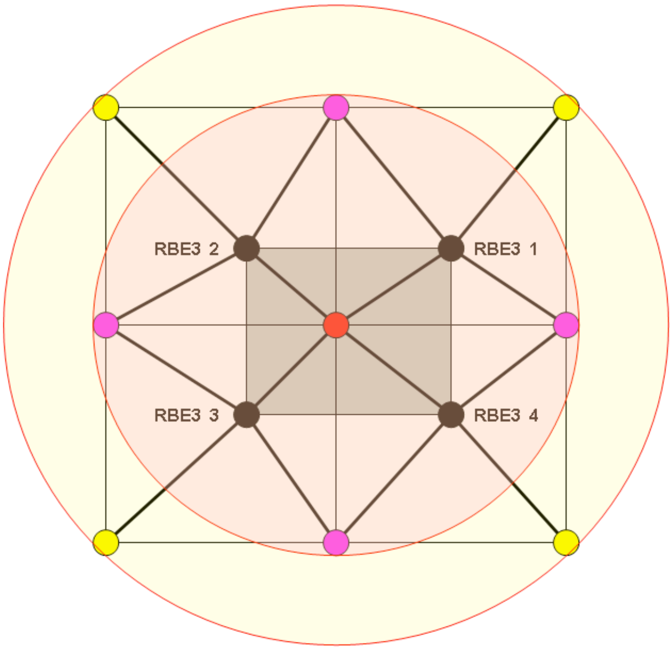

Figure 2.8: The radiating stiffness araound the ACM2 model

2.3 Literature review

Palmonella and Friswell [01, 06] define main requirements which a practical spot weld model should provide. The major demand is that the model should accurately represent the stiffness and mass characteristic of the real welds and their influence on the rest of the structure. Another demand is that the spot weld models should have a short modelling time. This goal is mainly determined whether the model requires congruent meshes of the two plates which are connected.
The spot weld models are not only represented by a nugget, the group of shell elements which are taking part are named as ”patch”. A single spot weld is build out of an upper and lower patch and a nugget element between. These involved patches have often strongly varying geometries and their areas are mainly influencing the stiffness of the whole structure.
The simplest models are single beam and brick models, which are also named as ”non-patch” like models. Single beam models consist of rigid or elastic beams, in the easiest case they are only represented by the connection of two coincident nodes. These models generally tend to underestimate the stiffness of the spot weld connections. For single brick models a solid element is used which is connected via rigid connectors to the nodes of the shell element. The rigid connections are responsible for the transfer of moments. Such models gave a good description of the local stiffness around the spot weld,

but they don't have suitable parameters for an updating process. But the main disadvantage of single beam and brick models are that non-congruently meshes couldn't be connected. So it is necessary to remesh around the spot weld center, which violates with the goal of a fast modelling time.

The most common spot weld approaches in NVH [01] are the ACM2 (area contact model 2) and the CWELD model. The ACM2 model is proposed from Heiserer et al. [03] it consist of a brick element which is connected via RBE3 elements with the upper and lower plate. The element is available in *MSC.Nastran* as well as the CWELD modelling approach. The CWELD has instead of a brick element for the nugget representation a special shear flexible beam-type element, with two nodes and 12 degrees of freedom (DOF). The 6 DOF's of the two beam ends are connected with shell nodes of the participated plates and form a patch.

In [01, 06] the spot weld models mentioned above were used to investigate sensitive parameters, which can be used to update and validate the finite element approaches. For this purpose a benchmark structure was constructed to achieve experimental data for the updating process. The benchmark structures have been a "single and a double hat" construction, which are steel plates who have in the cross section a form like a "hat". These plates are joined together at the flanges to represent for example a roof pillar of car body. The general intention of the approach in [01, 06] is to use measurement data of the benchmark structure to determine values of appropriate stiffness parameter. First the separate plates were tested and updated, so that the error which might occur in the welded structure is only due to the spot weld model itself. The benchmark structure is then updated only with the use of parameters which are involved in the spot weld approach. The investigated parameters are the patch area (PA), the patch size (PS, which is the square root of the area), the patch Young's modulus (PE), the spot diameter (SD) and the spot Young's modulus (SE).

The updating in [01] is performed with an optimisation algorithm implemented in the FE-code *MSC.Nastran*. The code specifies an objective function which is minimised and influences the output variables of the FE-analysis. In the present study only the eigenfrequencies are regarded and the objective function is described in [17].

In [01] it's shown that for the CWELD and the ACM2 model PA and PE are sensitive parameters and for the ACM2 additionally the spot diameter. In a common FE-model the patch has the same Young's modulus like the surrounded structure (i.e. for steel 210 GPa). The PA is dependent on the mesh size of the involved panels and SD is normally equal with the real nugget diameter. Palmonella [18] found out in experimental tests that the spot weld diameter doesn't influence the dynamic behaviour of the structure and therefore the eigenfrequencies. For CWELD and ACM2 an optimal patch size between 9 and 12 mm was shown. The assumption to use PE for compensation of not ideal patch size does only hold up to a PS of 12 mm, above PE and PS have different influence on the eigenfrequencies. For small values of PS the updating of PE leads to a decreasing difference between measured and calculated natural frequencies. But smaller patch sizes reduce the sensitivity of the eigenfrequencies to the patch parameter, which requires very large variations of the patch Young's modulus in the updating process.

In real structures the spot welds are mostly grouped in rows. Thus one can define two directions, one is ”longitudinal” which refers to the direction parallel to the spot weld row, the second direction is ”transverse” and perpendicular to the spot welds line. Tests in [01] show clearly that parameters like patch width, position of the spot weld, patch and spot shifts related to the transverse direction are much more important than in longitudinal direction. The reason is that the transverse direction significantly effects the stiffness property and hence the dynamic behaviour of the structure. Another not unimportant parameter is the thickness of the plates, which show up in the patch of the spot element. For variations in plate thickness the ACM2 model is a little bit less sensitive than the CEWLD.

In [01] a guideline is given for the CWELD and ACM2 models how to update them and minimise the difference between measured and calculated eigenfrequencies. For different plate thicknesses a optimum patch size (PS) is presented and the percentage change in the patch Young's modulus (PE) if below or above optimum PS. Using this updating approach for the ”single and double hat” structure welded with ACM2 and CWELD, the errors in the first 10 eigenfrequencies can be reduced in average to less than around 2%.

3 The benchmark structures

To produce experimental data which is necessary to validate the corresponding Finite-Element-models a suitable benchmark structure is needed. In this work the benchmark structure is a sidemember panel from a current Volvo car body. The sidemember is a bearing part in the engine compartment which has a large importance for crash safety. Therefore the sidemembers represent a quite stiff structure of the car with a nominal panel thickness between 1.8 and 2.0 mm. The complete sidemember installed in the car is built up with a so called inner sidemember and the corresponding outer part, which are both shown in pictures (3.1, 3.2).
The sidemembers are pressed metal panels which have a complex three dimensional shape with holes and curvatures. Both panels have dimensions in the width direction of ca. 21 cm at the short side and of ca. 54 cm at the long side. The inner and outer sidemembers have a length of approx. 109 cm and 84 cm.

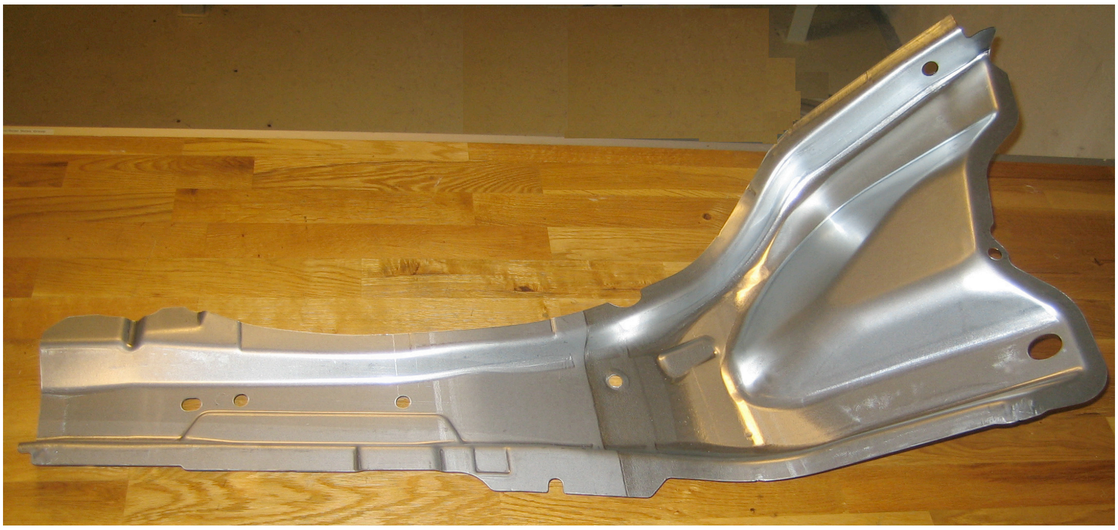

Figure 3.1: Single inner sidemember

Figure 3.2: Single outer sidemember

To form the sidemember "assembly" the outer panel is put on the top of the inner part, with the positions like demonstrated in the pictures (3.1, 3.2). The inner and outer sidemember panels are welded together with 49 spot welds which have a nominal diameter of 6 mm. The spot welds are positioned along the flanges of the assembled sidemember, which can be depicted in figure (3.3).

Figure 3.3: Welded sidemember (assembly)

4 Measurements

For validation purpose of the Finite-Element-models vibration measurements were performed with the use of the benchmark structure described in chapter (3).

4.1 Pre-Investigations

Based on the fact that the single sidemember panels and the welded assembly represent a very stiff test specimen investigations are done to find suitable excitation points on the objects. Due to this reason eigenfrequency analyses of the three different sidemember parts are made with *MSC.Nastran*. The calculated eigenfrequencies and eigenvectors are used to animate the related mode shapes in *Matlab*. With the help of these mode shape animations the areas with the highest displacements on the test objects are determined. These "sensitive" regions are used for the placement of excitation points to measure frequency response functions (FRF's). For all three sidemember parts the excitation points are later placed mainly on the flanges of the structures, because there the largest movements can be observed for the majority of the modes. This can be seen in the figures (4.1, 4.2) as an example for the mode shapes of the first eigenfrequency.

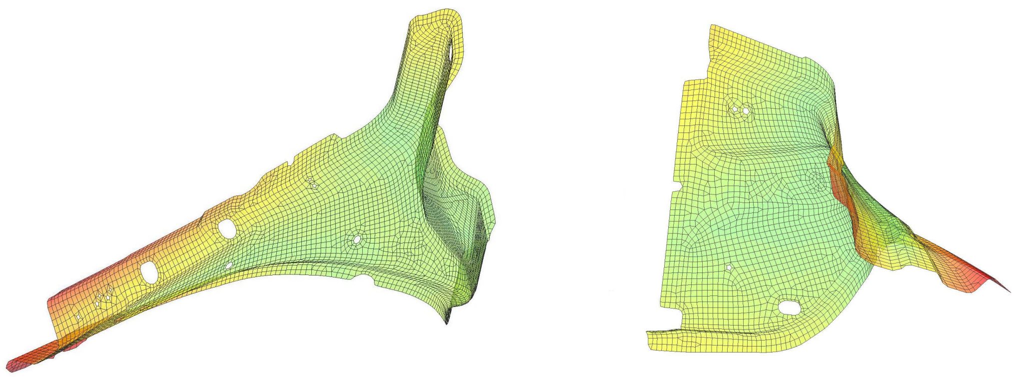

Figure 4.1: Mode shapes of the first eigenfrequency for the inner sidemember (left) and outer sidemember (right)

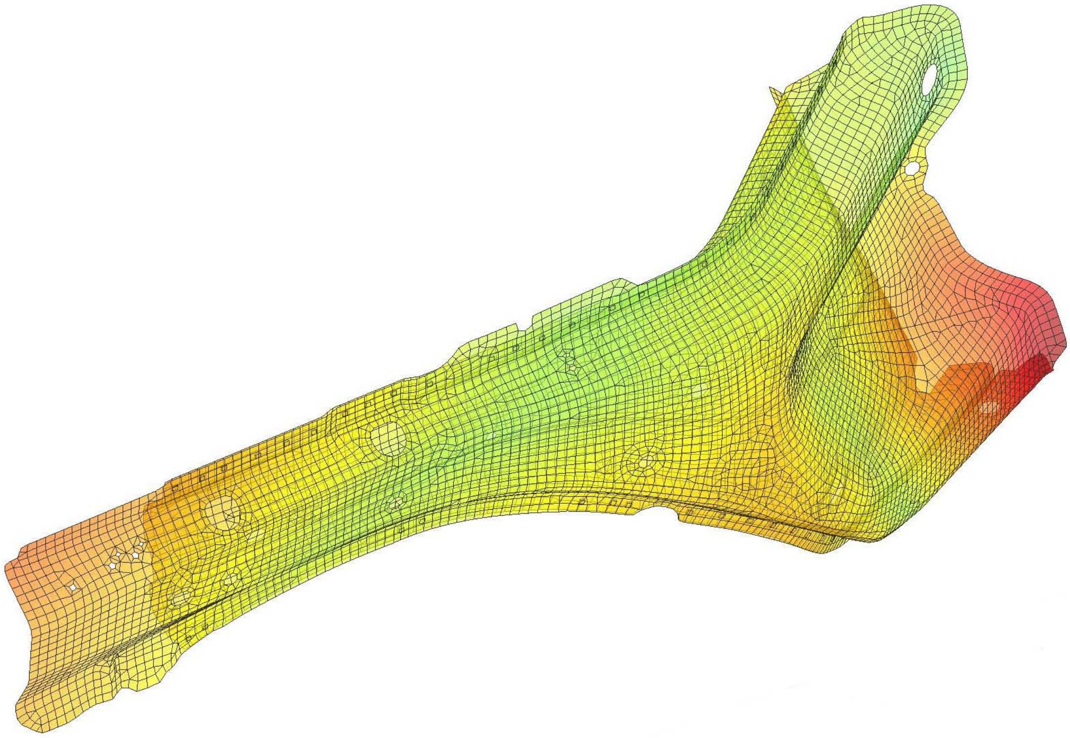

Figure 4.2: Mode shape of the first eigenfrequency for the welded assembly

4.2 Configuration

After the excitation points were chosen, the structure under investigation was hooked up with springs to achieve free-free conditions, which can be seen in picture (4.3). The excitation was done with a shaker which was connected via a stinger to the test object. All specimens were excited from the bottom side, so that the responses could be measured at the facing positions on the upper side. At five measurement points on each sidemember panel the Pointmobilities (PMOB) and the belonging Transfermobilities (TFMOB) were determined to get a complete FRF-matrix. All measurements were carried out in the frequency range between 0 and 1000 Hz and with the highest frequency resolution, which is available from the acquisition system. This is necessary to achieve a sufficient resolution especially at the resonances peaks of these very light damped structures.

Figure 4.3: Measurement Set-Up

4.3 Eigenfrequencies & Damping

The measured mobility's, like described in (4.2), were used to determine the eigenfrequencies and the modal damping of the sidemember parts. For this purpose the Complex Exponential Method was selected, like described in [13]. The viscous damping factor (ξ_r) was transferred in the loss factor (η_r) to have later an estimation value for the Direct Frequency Response Analysis in *MSC.Nastran*. But the main focus in this work was set on the determination of the eigenfrequencies from measurements. With the use of the measured Pointmobilities the eigenfrequencies were extracted. For each sidemember set with three specimens an averaging process was performed, to obtain "mean" eigenfrequencies for the inner & outer sidemembers and the welded assembly. These "mean" measured eigenfrequencies will be compared later in this work directly with the FE-simulations. In table (4.1) the "mean" eigenfrequencies are presented for the inner & outer sidemember and the welded assembly.

Mean Eigenfrequencies			
Nr.	Inner [Hz]	Outer [Hz]	Assembly [Hz]
1	22.65	31.27	68.19
2	51.94	42.06	110.11
3	88.42	95.65	135.74
4	112.71	133.52	161.45
5	148.67	149.08	201.22
6	181.03	178.30	231.19
7	200.67	225.64	235.54
8	217.78	246.61	259.05
9	227.08	292.26	—
10	267.75	—	—

Table 4.1: "Mean" measured eigenfrequencies for the inner & outer Sidemember and the welded assembly

4.4 Deviation for the sets of the three sidemember parts

All three test specimens which belong to the set of an inner & outer sidemember and welded assembly were measured individually, to see if there are significant deviations in a set, caused for example by the production process. Therefore the resulting eigenfrequencies, masses and FRF's of the three test objects in a set will be compared to each other.

Eigenfrequencies

In a first step the deviations in percent between the eigenfrequencies of the three sidemember sets were observed. The results are shown in table (4.2). This table shows that for both sets of the single sidemember parts the deviation in the eigenfrequencies is in average less than 0.5 %. This shows that there is a high accuracy and reproducibility during the metal forming process, where the flat metal sheets are pressed and cut in the desired shape. For the set of welded assemblies the deviation is slightly increasing up to an average of ca. 1%. But this behaviour was expected because the spot weld positions are slightly differing between the three assemblies. The reason therefore is that the single panels were welded together in the prototype plant and not in the production line.

Deviation in Eigenfrequencies			
Nr.	**Inner [%]**	**Outer [%]**	**Assembly [%]**
1	0.3	0.4	1.3
2	0.3	0.3	0.3
3	0.1	0.1	1.2
4	0.1	0.1	0.9
5	0.1	0.2	1.0
6	0.4	0.3	0.2
7	0.2	0.1	0.8
8	0.5	0.3	1.1
9	1.0	0.2	—
10	0.1	—	—

Table 4.2: Deviation in eigenfrequencies for the sets of inner & outer sidemember and the welded assembly

Masses

In a next step the "real" mass of each panel or assembly was determined to see the largest deviation in each set of the three sidemember parts. The results are presented in table (4.3), where one can observe that the maximum deviation is less than 22 g for all three sidemember sets.

Outer	Panel 1	**4.342 kg**
	Panel 2	**4.350 kg**
	Panel 3	**4.349 kg**
max. deviation		**8 g**
Inner	Panel 1	**6.277 kg**
	Panel 2	**6.293 kg**
	Panel 3	**6.295 kg**
max. deviation		**18 g**
Welded	Assembly 1	**10.625 kg**
	Assembly 2	**10.647 kg**
	Assembly 3	**10.639 kg**
max. deviation		**22 g**

Table 4.3: Deviation in mass for the sets of inner & outer Sidemember and the welded assembly

Annother interesting comparison is presented in table (4.4). There the measured masses of all three inner and outer sidemembers were summed up and compared with the corresponding measured masses of the assemblies. The resulting differences indicate that the welding process itself didn't influence the mass of the structures significantly. These small mass deviations are negligible and confirm with the observations made for the eigenfrequencies.

assembly	measured [kg] sidemember inner	measured [kg] sidemember outer	sum [kg]	measured [kg] welded assembly	diff [g]
1	6,277	4,342	10,619	10,6245	**5,5**
2	6,293	4,350	10,643	10,6469	**3,9**
3	6,295	4,349	10,644	10,6391	**-4,9**

Table 4.4: Comparison of mass deviation after welding process

FRF's

To see if there are significant deviations over the entire frequency range of interest, measured FRF curves were compared.

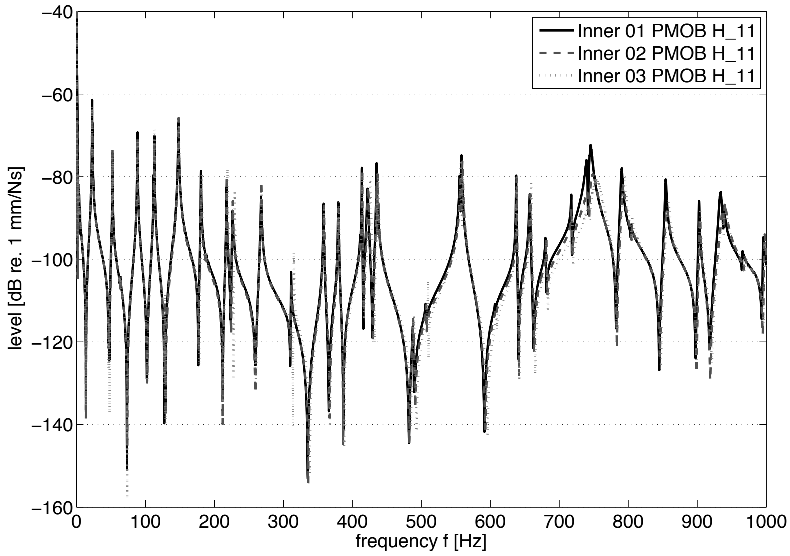

Figure 4.4: Comparison of Pointmobilities of the inner sidemember

As representative examples the Pointmobilities of the inner sidemembers at measurement point 1 and of the welded assemblies at measurement point 3 were chosen, which are illustrated in figures (4.4) and (4.5). There it gets obvious that all three Pointmobility curves show only small differences, even up to 1000 Hz.

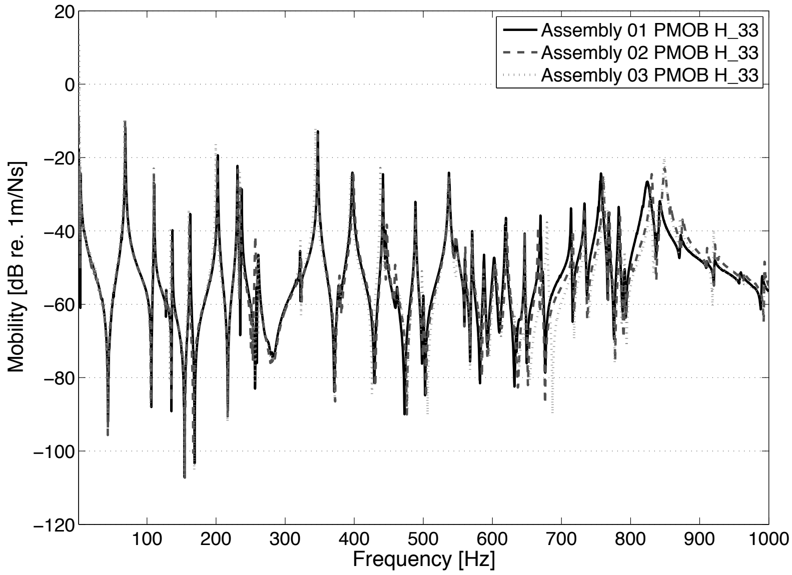

Figure 4.5: Comparison of the measured point mobility on all individual assemblies

These insignificantly deviations in eigenfrequencies, masses and FRF's in each set of the three sidemember parts are a indicator for the precision during the production process and just so for the performed measurements. This confirms the procedure to determine "mean" eigenfrequencies for each set of the sidemember parts and to calculate also a mean FRF for comparison with the corresponding FE-calculations.

5 Single sidemember panels

In this chapter measured FRF curves and eigenfrequencies of the single sidemember panels will be compared with the relevant FE-simulations. The FE-calculations were performed with the FE-solver of *MSC.Nastran*. For the calculation of the eigenfrequencies the Real Eigenvalue Extraction was chosen, which uses the Lanczos Method and is defined with the solution number SOL 103 in *MSC.Nastran*. The frequency response analysis was done with the Modal Frequency Response Method, which is selected with SOL 111. Both solution methods are described in detail in the Basic Dynamic Analysis manual [20] of *MSC.Nastran*.
The sidemember panels were modelled with shell elements, using exclusively quadrilateral plate elements and in some small areas triangular shell elements. These are CQUAD4 and CTRIA3 elements in *MSC.Nastran* 2005 and described in the Quick Reference Guide [20].

5.1 Mesh refinement

All following investigations concerning the single sidemember panels are described exemplarily with the inner sidemember because the results for the outer panel are mainly identical. If there are any significant differences occurring, explicit statements will be made.
At the moment the quadrilateral elements have a "standard" mesh size of 10 mm and a linear shape function. At this point it should be stated that one of course can use higher order shape functions instead of refining the mesh to achieve the same or similar effect. But in the automotive industry it is usual to use the same meshes for Durability, Crash and NVH to safe time and costs. Especially for crash simulations linear shape functions are absolute necessary, so that they have to be used for NVH purpose as well. In this work the 10 mm mesh is the "reference size" and in addition three smaller mesh sizes were investigated, which are 5, 2.5 and 1 mm. The inner sidemember panels have two areas with a nominal thickness distribution of 1.8 and 2.0 mm.
In figure (5.1) one can see for the inner panel the FE-calculations for the 10 and 1 mm mesh and the corresponding mean measured curve. There it gets obvious that it is hard to recognize the differences in eigenfrequencies in such a FRF plot.

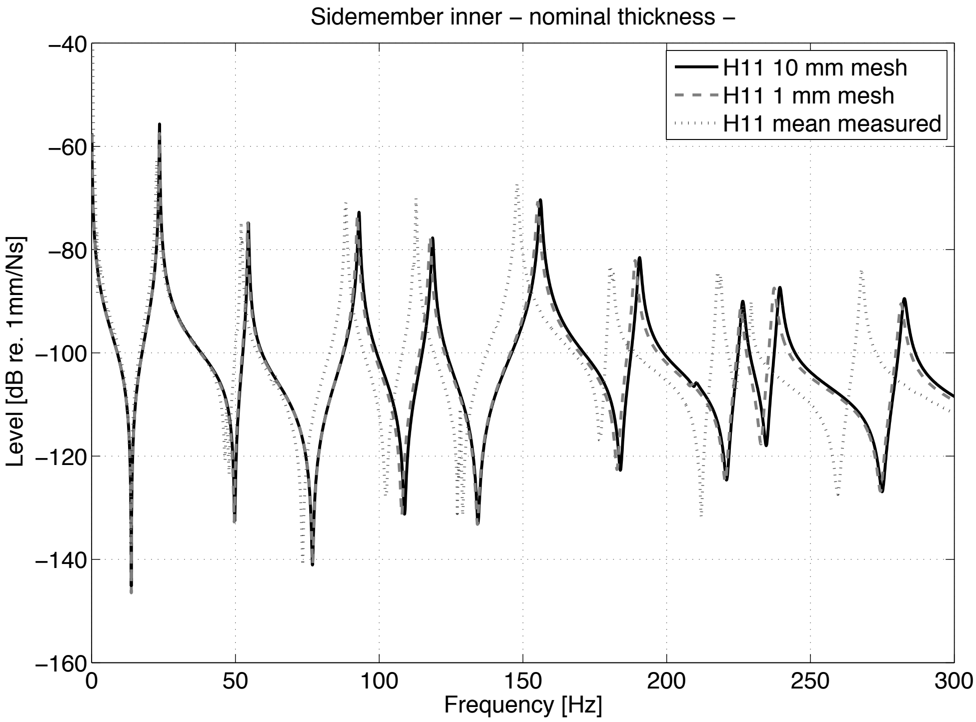

Figure 5.1: Moblity curves for the inner sidememeber with a mesh size of 10 and 1 mm and the corresponding mean measured curve

Even for the largest difference between 10 and 1 mm and a reduced frequency range from 0 to 300 Hz, it's necessary to zoom in a single resonance to detect differences. This way of graphical presentation is shown in figure (5.2) exemplary for the resonance frequency at around 150 Hz and all used mesh sizes. But even with this extensive procedure it's almost impossible to make these small differences visible, so it was decided to chose for further comparisons a bar plot which shows the differences in percent between FE-calculations and measurements for all modes up to 300 Hz. Such a bar plot is illustrated in figure (5.3) for the inner sidemember. There one can now clearly see the deviation between measurement and FE-calculation for the first ten modes of the inner panel. With this kind of graphic the influence of each mesh refinement step can be detected and the efficiency estimated. For the inner panel the first mesh refinement from 10 down to 5 mm shows the largest effect and the improvement for the first ten modes is in average around 0.5%. Looking on the same graphic for the outer sidemember in figure (A.1) of the appendix, one can see for the same refinement step from 10 to 5 mm a larger improvement than for the inner panel.

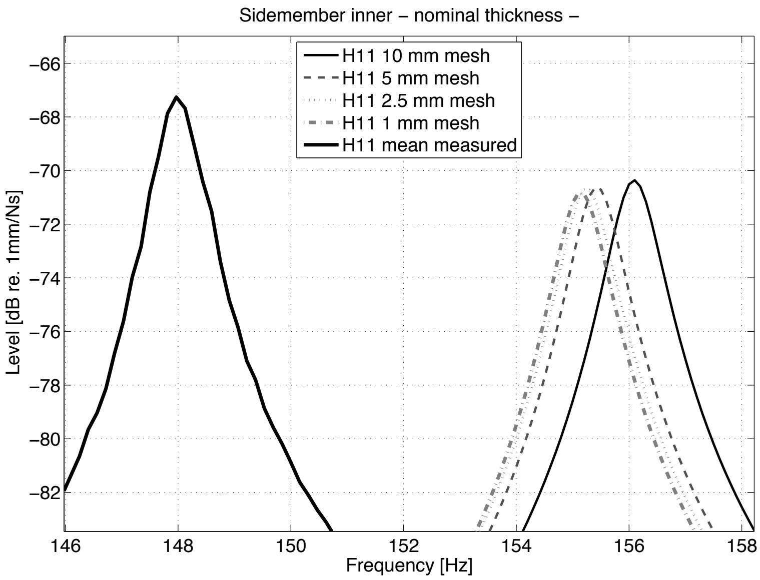

Figure 5.2: Zoom view of a resonance frequency at around 150 Hz

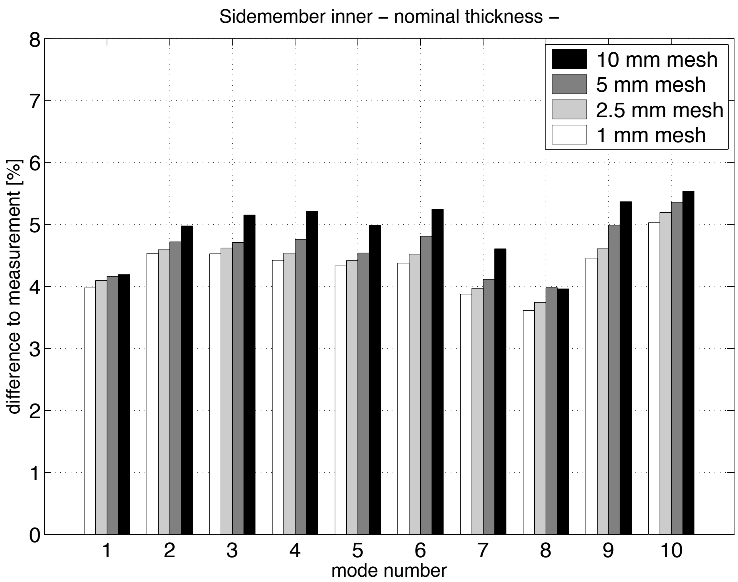

Figure 5.3: Differences in eigenfrequencies for the first ten modes of the inner sidemember, due to mesh refinement

To make the influence of this first refinement step more visible, the arising difference in Hz due to refinement is plotted for a larger frequency range up to around 750 Hz in figure (5.4). There it can be observed that the inner and outer sidemember show a really different behaviour due to refined panel meshes. The outer panel is much more sensitive because of refining the mesh. In general it can be stated a highly mode depend sensitivity.

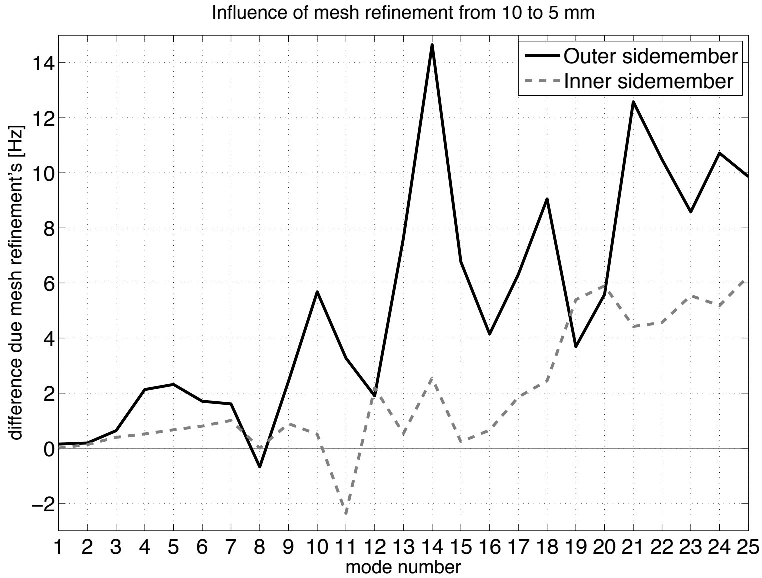

Figure 5.4: Difference in Hz for the first 25 modes of the inner and outer sidemember, because of refined mesh from 10 to 5 mm

To find reasons for this behaviour one has to think about the Finite-Element-Method itself. There it's known that the FEM is an approximation method, which discretizes a structure in a finite number of points (nodes). With a finer mesh one achieves a higher number of nodes, which means a more detailed discretization of the geometry behind the structure. If the structure is highly complex and three dimensional, like in our case the sidemembers are, one gets with a growing number of nodes also a better mass representation at these nodes. This can also be observed in the mass of the model when refining the mesh density. Table (5.1) shows the mass development for the inner sidemember with nominal thickness distribution with increasing mesh density.

Inner sidemember mass development [kg]				
mesh density	10 mm	5 mm	2.5 mm	1 mm
nominal	6,712	6,730	6,734	6,736
measured	6,288	6,288	6,288	6,288
Difference	0,423	0,442	0,446	0,447

Table 5.1: Mass development when refining the mesh density with nominal thickness

It can be seen that the increasing mesh density leads to an small increasing mass of about 24 g because of a better approximation of geometry (curvatures and holes). This at least results in a small drop in eigenfrequencies. The mass then directly influence the calculation of the eigenfrequencies and the mode shapes, which are moving nearer to the measured (”reference”) values. In figure (5.4) one can observe that the convergence step of the eigenfrequencies to the ”real” value is stronger with growing frequency. A reason therefore is that with higher frequencies and shorter wavelength fine details in geometry, like small holes and edges, affect stronger the vibrational properties of the structure. In figure (5.5) the same geometry area is shown, once with the standard mesh size of 10 mm and then with the finer mesh size of 2.5 mm. There the effect of the better geometry approximation gets directly visible. At the end the change of the considered eigenfrequency due to a refined panel mesh depends only on how good the standard mesh could represent the geometry and the occurring bending stiffness at this specific frequency under investigation.
For the single inner and outer sidemember panels the first refinement step from 10 to 5 mm has the largest effect in reducing the deviation between measured and calculated eigenfrequencies. With this first step an improvement in the eigenfrequencies of ca. 0.5% could be achieved for the first ten modes. Both next refinement steps from 5 to 2.5 mm and 2.5 to 1 mm, change the eigenfrequencies in average only about 0.1%.

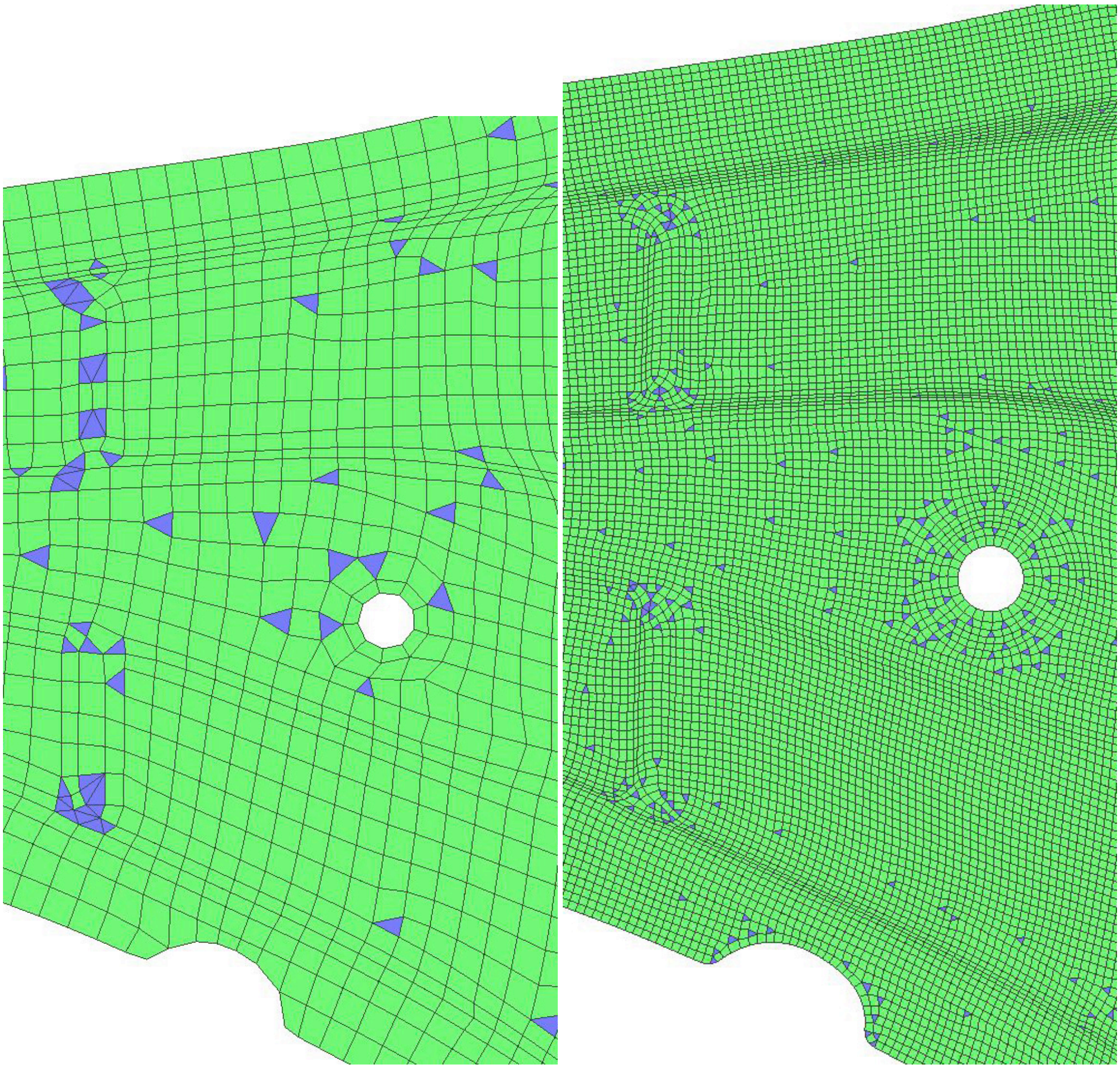

Figure 5.5: The same geometry with standard 10 mm mesh (left) and refined mesh with 2.5 mm (right)

5.2 Mapped thickness distribution

After refining the mesh size a detailed thickness distribution over the surface of the panels was tested. This detailed thickness information's come from the metal forming process where the originally flat metal sheet is pressed in the desired shape. To examine this pressing process also FE-simulations are performed, to check that no possible fracture zones appear. These metal forming simulations contain the actual height of the panel at each node.

In figure (5.6) such a mapped thickness is presented for the inner sidemember panel. There it can be seen that the inner panel has two parts with different initial heights. The left side has a starting height of 1.8 mm and the right side of 2.0 mm. Due to the pressing process the maximum height difference can be more than 0.5 mm on this single panel. It is also possible that the thickness of some areas increase above the initial height because the metal moves under the high pressure; like for the right side of the inner panel. But over the whole panel a noticeable variation in height gets visible.

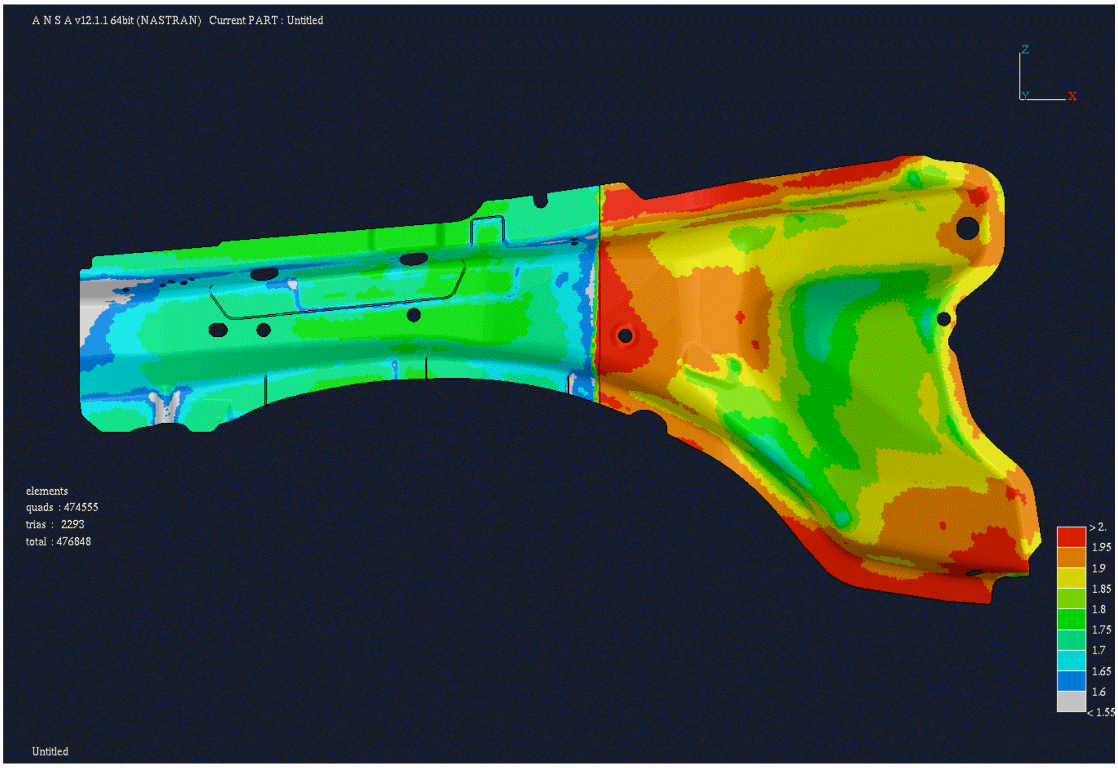

Figure 5.6: Mapped thickness distribution for the inner sidemember

Previous FE-simulations neglected this existing effect of mapped thickness. In the following FE-calculations the mapped thickness was implemented into the present meshes, to see how they influence the dynamic properties of the sidemember parts.

In figure (5.7) the 10 mm standard mesh is compared with nominal and mapped thickness, additionally the mesh refinements of 5 and 2.5 mm for the mapped thickness are illustrated. There it gets obvious that with the consideration of the real thickness the deviation in eigenfrequencies between measurement and FE-calculation can be reduced in average for the first ten modes of the inner panel by ca. 3%. The expected differences due mesh refinement appear in the same order as for the nominal thickness. Now the question came up, what are the reasons for such a large improvement caused by mapping.

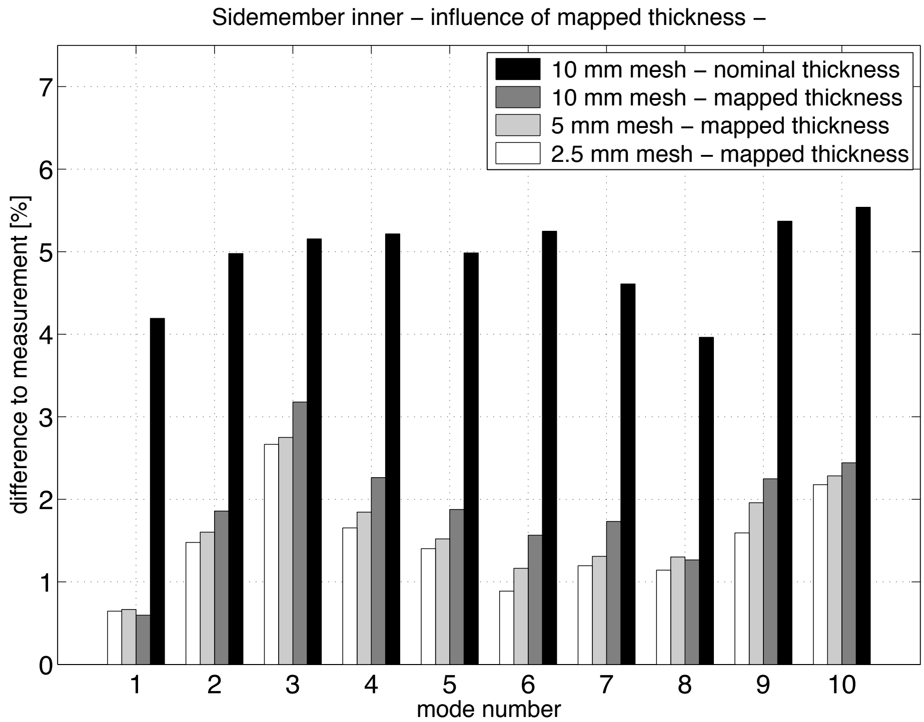

Figure 5.7: Comparison of eigenfrequencies with nominal and mapped thickness for the inner sidemember

First the mass development of the FE-models for the inner sidemember was investigated, like shown in table (5.2).

Inner sidemember mass development [kg]				
mesh density	10 mm	5 mm	2.5 mm	1 mm
mapped	6,311	6,331	6,336	6,338
measured	6,288	6,288	6,288	6,288
Difference	0,023	0,043	0,048	0,050

Table 5.2: Mass development when refining the mesh density with mapped thickness

There one could find a mass reduction of 373 g between the 10 mm standard model with nominal thickness and the 1 mm mapped model. The mass of the models is converging down and is with the 1 mm mapped model only 50 g above the "real" weighted mass. Generally a decreasing mass leads to increasing eigenfrequencies, but figure (5.7) shows the opposite behaviour. If not the change in mass is responsible for the shifted downwards eigenfrequencies, it has to be the changed thickness itself. Therefore the behaviour of the bending wavelength for a simple quadratic plate was chosen, which can be calculated like follows:

$$\lambda_B = 2 \cdot \pi \sqrt[4]{\frac{E \cdot h^3}{12\,(1-\mu^2) \cdot m' \cdot \omega^2}} \tag{5.1a}$$

$$\lambda_B = 2 \cdot \pi \sqrt[4]{\frac{E \cdot h^3}{12\,(1-\mu^2) \cdot h \cdot \rho \cdot \omega^2}} \tag{5.1b}$$

With equation (5.1b) two cases were calculated, first reducing the thickness of the plate from 2.2 mm down to 1.7 mm and then changing the density to achieve the same mass reduction like with the reduced thickness by 0.5 mm. The resulting changes in frequency for three observed frequency points are presented in table (5.3).

observed frequency points [Hz]	**Δf [Hz] when changing thickness h**	**Δf [Hz] when changing density ρ**
200	-45	28
400	-81	55
600	-136	83

Table 5.3: Frequency steps due to changing thickness or density

There it gets evident if changing the thickness the eigenfrequencies are decreasing and the plate becomes "weaker". If adjusting the density a "stiffening" of the plate is visible and the eigenfrequencies are increasing. If simplifying equation (5.1b), with eliminating the thickness in the denominator, which comes from the calculation of the mass per area, the thickness in the numerator has still the power of two. So it is obvious that for the bending wavelength and therefore also for the eigenfrequencies the thickness of the structure is the dominating parameter. With these mapped thickness distribution one gets a much better representation of the reality than with using a nominal thickness over the whole panel area. And since the thickness of a structure is dominating its bending stiffness behaviour, the deviation between measured and calculated eigenfrequencies can be reduced significantly with the use of mapping. This gets also visible when comparing FRF curves, like in figure (5.8). There one can see a direct comparison between nominal and mapped thickness distribution and as a reference the corresponding measured curve. With growing frequency the improvement due to mapping gets larger, which is detailed illustrated for an extended frequency range in the appendix (A.2).

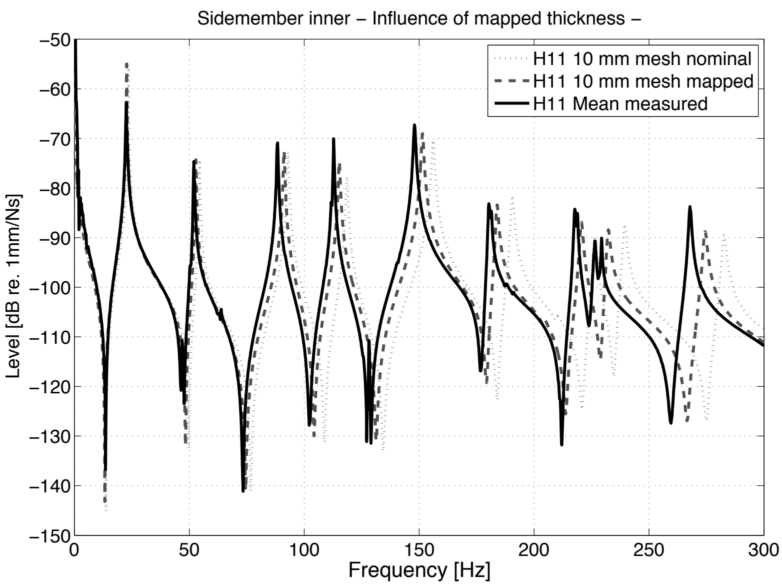

Figure 5.8: FRF comparison to show the influence of mapping

5.3 Main results

To improve the FE-model with the complex geometry of the single sidemember panels a mapped thickness distribution was introduced. This leads to a reduction of the deviation between measured and calculated eigenfrequencies of ca. 3%. In contrast to a simple Young's Modulus updating, the improvement due mapping works nearly uniformly for all modes in the frequency range up to 300 Hz. The mapped thickness reduces the error between eigenfrequencies from measurements and FE-simulations for the first ten modes of the single sidemember panels to less than 2% in average.

In another investigation the standard mesh size of 10 mm was refined down to 5, 2.5 and 1 mm. To see the influence of this three refinement steps, the change of the eigenfrequencies in Hz for the inner and outer sidemember was averaged and plotted in figure (5.9) for the first 25 modes, which cover a frequency range from 0 up to ca. 750 Hz.

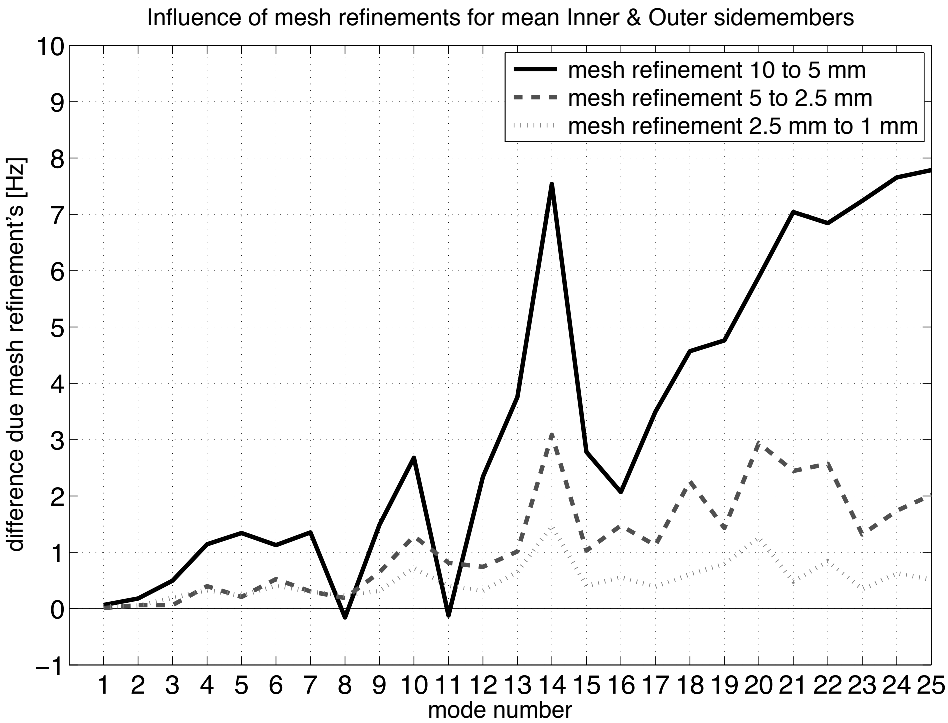

Figure 5.9: Change of eigenfrequencies in Hz for all three refinement steps

An interesting observation is that a few modes show a strong reaction or are insensible at all in consequence to a finer mesh. Insensibility means that the "rough" mesh was already sufficient to describe this single mode. Instead a strong reaction shows the

requirement of finer mesh size. But in general the largest improvement can be achieved with the step from 10 to 5 mm mesh size.
Up to 300 Hz this leads to an improvement of the FE-calculated eigenfrequencies of ca. 0.5%, but the tendency is that the improvement increases with frequency. So it depends on the frequency range of interest if the refinement from 5 to 2.5 mm is useful or not. The refinement step from 2.5 mm to 1 mm changes the eigenfrequencies only about 1 Hz for all 25 modes under investigation, but the calculation effort is increasing exponentially. So this case, with refining the panel mesh down to 1 mm is inefficient and not recommendable.

6 Investigations of welded assembly

After the investigations on the single sidemember parts, the welded structure has to be modeled. Due to the welding process the global stiffness of the assembly is now determined by the bending stiffness of each single members but mainly of the stiffness of the spot weld connections [07]. After joining the single side members together, the exact spot weld positions were determined with the help of a special laser system for all three assemblies. With the laser measurement data it is possible to implement the spot weld models in the FEM model exactly at the same position. In figure (6.1) one can see the 49 spot weld positions which are marked as black square elements.

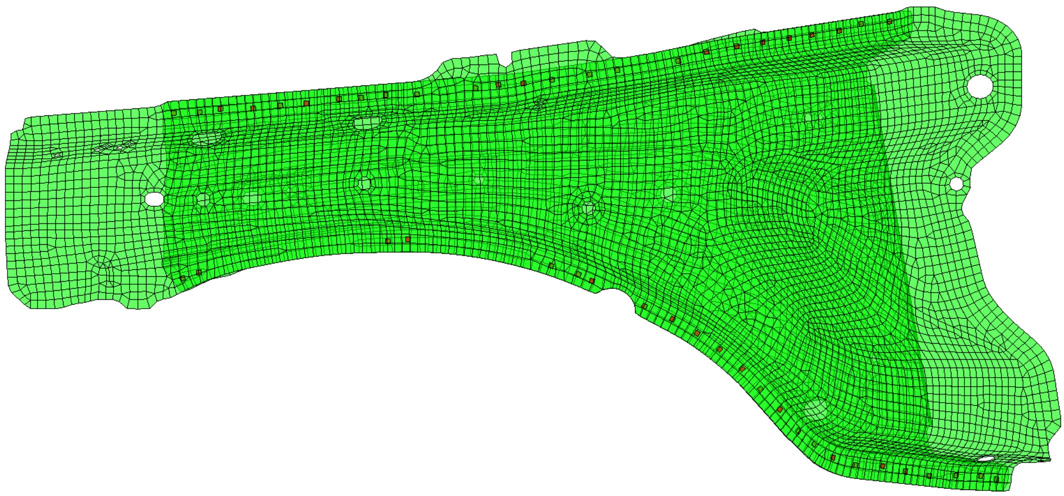

Figure 6.1: FEM model of welded assembly with black marked spot weld positions

6.1 ACM2 vs. CWELD

As mentioned in [05] the most widely used spot weld models in industry are the ACM2 and CWELD model. In a first investigation simulations with both models have been carried out to be able to compare the performance of both models concerning to further mesh refinement. Therfore the standard models with an spotweld diameter of 6 mm have been used. Figure (6.2) shows the results for mesh refinement steps from 10 mm down to 2.5 mm.

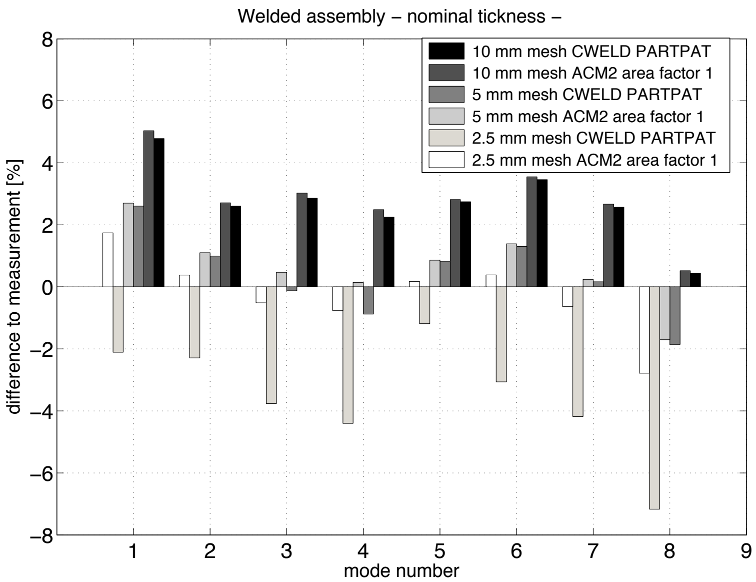

Figure 6.2: Difference between measured and calculated natural frequency for the different models [%]

With a 10 mm mesh the CWELD and the ACM2 model performs quite similar. When going down to 5 mm mesh size the CWELD model begins to loose more stiffness especially at mode number 3 and 4. Here the ratio D/S becomes larger 1 which leads to an underestimation of the connection stiffness. This effect becomes larger with a meshsize of 2.5 mm. But there occured also an another difficulty. Due to the fact that the CWELD model is only able to connect from 1 up to 3x3 shell elements, the spotweld diameter has also to be reduced. Now a second factor, the spot weld diameter additionally influences the connection stiffness.

As mentioned in [01] the spot weld diameter is not a sensitive parameter for the CWELD model, but decreasing the diameter includes also a reduction of the connected patch area, especially at small mesh sizes. The patch area again is of course a sensitive parameter as well as for the ACM2 model.

Although both models loose stiffness with further mesh refinement, the CWELD model performs worse because of its functional limitations. It becomes clear that to compensate the loss in bending stiffness due to mesh refinement the CWELD will be more difficult to control. This is mainly because the only sensitive parameter in the PWELD entry which is possible to change, is the spot weld diameter. This shows that in general the CWELD model is not applicable for mesh sizes smaller than 5 mm. As a consequence further investigations have been done with the ACM2 model.

6.2 ACM2 model

As mentioned in chapter (1) the ACM2 model leads to a drop of global stiffness in the FEM calculation when refining the meshsize. The difficulty on the current model is of course that further mesh refinement itself leads as well to a drop of stiffness because of the better approximation of geometry. The coarsest mesh size for all investigations is a 10 mm mesh. Therefore it is important to find out an optimal spot weld configuration, which doesn't introduce any additional error in the simulation results. With a 10mm mesh the simulation results from the single sidemembers with nominal thickness have shown at the first 8 mode numbers a mean deviation of approximately 5 %. Normally the same quantity should also occur on the welded assembly with 10 mm mesh, if the applied spotweld model doesn't introduce any significant error from the beginning. In [01] Palmonella stated following sensitive parameters for the ACM2 model:

- Patch area (the area which encircles all connected shell elements)
- Patch Young's modulus
- Spot weld diameter (size of the brick element)

The patch area depends from the used mesh density, the Patch Young's modulus is not really a parameter which is practical to change, because the amount of elements which have to be updated changes with the used mesh density. The easiest possibility is to change the brick dimensions (spot weld diameter), because this parameter is mesh independent. To find out the optimal ACM2 configuration for a 10 mm mesh, several area factors have been investigated.

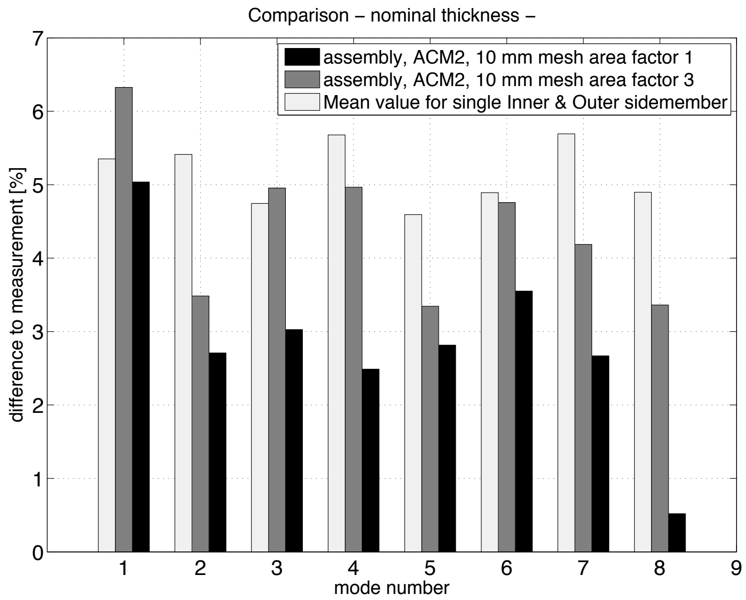

Figure 6.3: Comparison of area factor 1 and 3 with the mean deviation of single panels

Figure (6.3) shows, that area factor 3 (af3) is the best choice where the difference between the mean deviation of the single panels and the welded assembly becomes minimal. With area factor 3 the spot weld diameter was increased from 6 mm up to 9 mm. This configuration corresponds also to the standard model used at Volvo.

Of course there is still a difference between the welded assembly with af3 and the values of the single panels. One reason therefore is that the patch area of each individual ACM2 model is not the same on the panels. Wether on the whole panel nor the upper and the lower patch of one ACM2 model have the same patch area. One reason therfore is, because due to the complex shape of the structure some shell elements are distorted from their basic shape. Another reason is the location of the brick element inside the mesh. The largest patch area arises if each corner node of the brick element is lying in a separate shell element. Due to the complexity of the whole structure no ideal condition is given for each spot weld model. This of course affects individually the local bending stiffness of the structure. One can guess that these local variations in bending stiffness will more affect local base modes than global modes on the structure. Perhaps a compensation of such effects is only possible when updating only these ACM2 models whose stiffness is mainly responsible for a particular mode. But this effort would be too high in comparison to the achievable improvement.

With this initial spot weld model for a 10 mm mesh density, it was now possible to study further mesh refinement steps to quantify the loss in stiffness which is first of all caused from the mesh refinement and for another from the ACM2 model. Therefore all mesh refinement steps from 10 mm down to 1 mm have been calculated. Figure (6.4) shows the deviation in percentage between the different mesh models and the measured resonance frequencies.

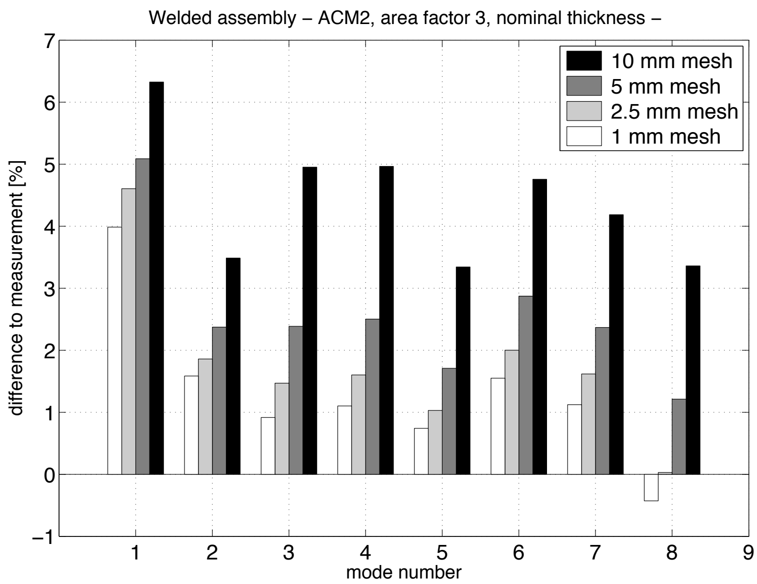

Figure 6.4: Difference of eigenfrequencies between simulation and measurement in % for nominal thickness distribution

In comparison to the simulation results for the single sidemembers with nominal thickness with further mesh refinement the deviation to measurement becomes too small. For the welded model normally one could expect the same order of size of approximately 5% for the first 8 mode numbers. This result shows clearly that the ACM2 model itself has a significat influence to the bending stiffness of the structure with further mesh refinement. Like mentioned before, the main problem is, that two effects are responsible for that stiffness loss. This is a better approximation of geometry and also the influence of the ACM2 model. Figure (6.5) makes the contribution of both effects independend from each other visible. The solid curve shows the mean change in frequency for the single panels when refine the mesh from 10 mm down to 5 mm. The dashed curve represents the change in frequency for the welded assembly with the same refinement step.

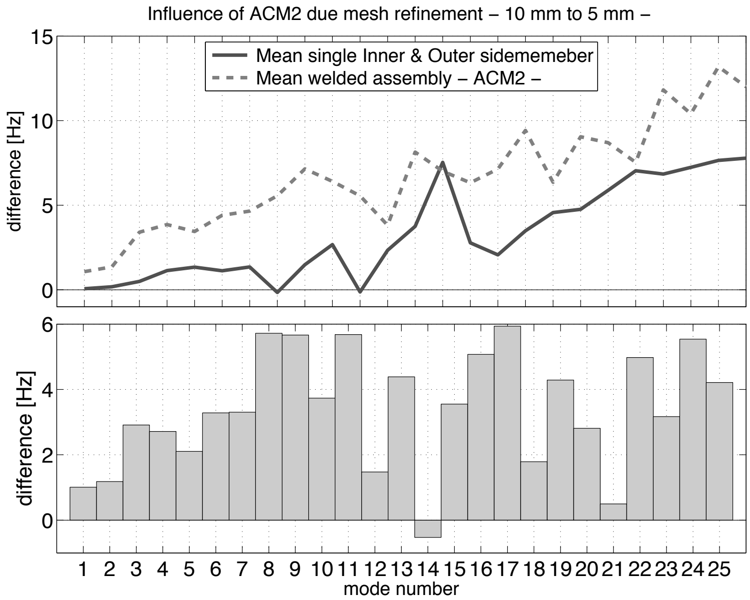

Figure 6.5: Change in frequency with mesh refinement from 10 mm to 5 mm for the first 25 mode numbers

One can see that the welded assembly shows a higher change in frequency like the single sidemembers. The area between both curves represents so to say the influence in frequency, for which only the ACM2 model is responsible for. The bar plot below shows this difference for each mode number. It can be seen, that the influence of the ACM2 models is mode dependend. This emphasizes the discussed influence of different patch areas of the individual ACM2 models to global and local modes.

Another investigation in [06] gives also a good explanation for mode dependency of this stiffness loss. There the different forces and moments acting at the spot welds have been analysed. It has been shown that a sensivity parameter like the patch area has the largest influence to those modes where the push / pull forces and bending moments are high in comparison to the shear forces. This means that the patch area has a larger stiffening effect to bending motion than for in-plane deformations. It is obviously that a reduction of the patch area by factor 4 due to mesh refinement has a higher affect to the bending stiffness of the whole structure than to the shear stiffness.

6.3 Reasons for stiffness loss with mesh refinement

To get a more detailed look on what happens, with further mesh refinement, one has to observe a single ACM2 model in the welded assembly. In figure (6.6) there is drawn a topview of an ACM2 model, before and after mesh refinement from 10 mm down to 5 mm. It can be seen that with one refinement step the patch area is reduced by factor 4. Another fact is, that the center of the brick element and thus the center of highest stiffness is not existing anymore, because the origin connection pattern of the whole ACM2 element is lost.

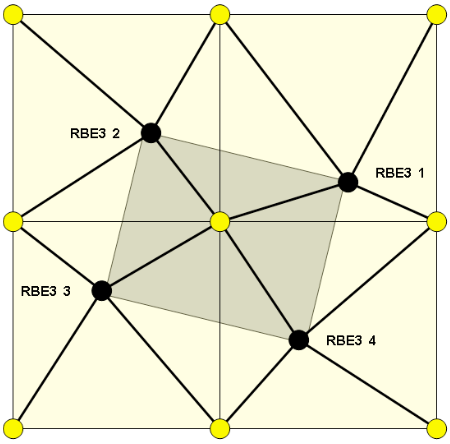

(a) origin ACM2 model

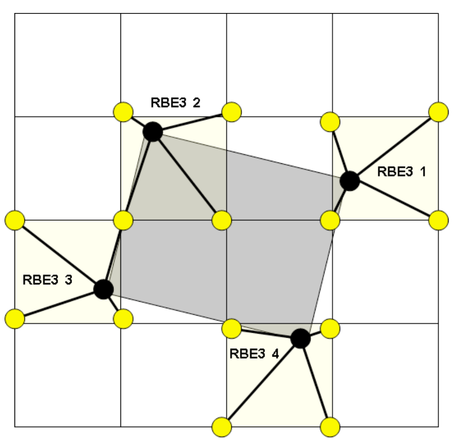

(b) ACM2 model after mesh refinement

Figure 6.6: Topview of an ACM2 model when refining the mesh density from 10 mm down to 5 mm

The answer for that lies in the implementation alghorithm for the ACM2 model. When connecting both sidemembers togehther the Pre-Processor tries to connect each of all 4 RBE3 points with those shell elements the RBE3 points are lying inside. However the originally ACM2 construction includes that not more than 4 shell elements are falling inside the brick area. Otherwise the origin connection pattern of the corner nodes will be lost.

6.4 Influence of mapped thickness distribution

As the previous investigations on the single panels have shown, with mapped thickness distribution the mean deviation in percentage between the measured and calculated resonance frequencies is about 2 % for the first 8 mode numbers. This means that when eliminating the error introduced by the ACM2 model the applied mapped thickness distribution on the welded assembly the deviation to measurement should result in the same order of size. Now the question arised, if the mapped thickness distribution has the same influence on the welded structure. Because when both single members are joined together a new structure arises and thus other geometrical properties could overcome the influence of mapping. Therefore the same mesh refinement steps from 10 mm to 1 mm have been calculated. In table (6.1) one can see the mass development for the welded assembly for all mesh refinement steps. It shows clear that even the coarsest mesh size approximates the real mass of the structure quite well.

Assembly mass development [kg]				
mesh density	10 mm	5 mm	2.5 mm	1 mm
mapped	10,569	10,615	10,634	10,638
´measured	10,637	10,637	10,637	10,637
Difference	-0,068	-0,022	-0,003	0,002

Table 6.1: Mass development for the assembly with mapped thickness

Figure (6.7) shows the deviation between the measured and the calculated resonance frequencies. One can see that with further mesh refinement the calculated resonance frequencies are now almost below the measured ones. This means that the structure becomes too weak in comparison to the real one. In comparison to the nominal thickness distribution in figure (6.4) the mapped thickness distribution has still a significant influence even if the structure is joined together. But now the influence of the ACM2 model is responsible for the fact that the bending stiffness of the FEM model is too weak. Due to the fact that the mapped thickness distribution has still a positive effect to the calculation results, further investigation were carried out with mapped thickness distribution.

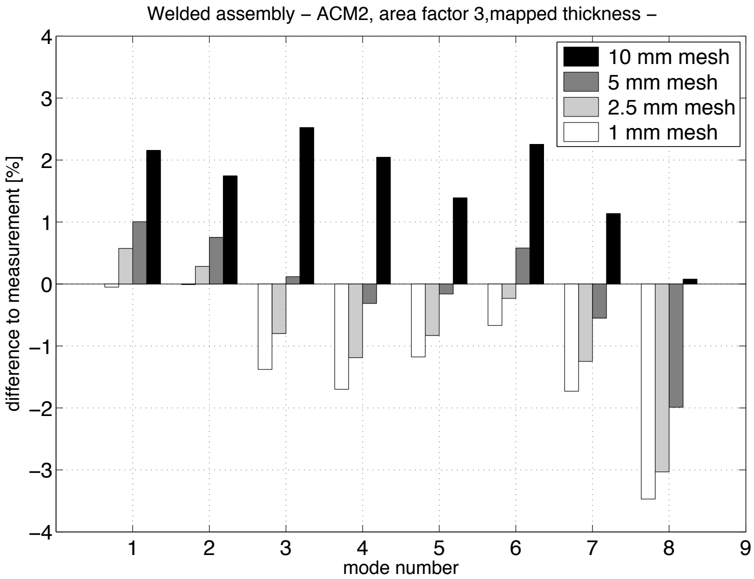

Figure 6.7: Difference between calculated and measured natural frequency in % with mapped thickness distribution

6.5 "RBE3 expansion" on ACM2 model

Based on a *Matlab* code written at Volvo, there is a possibility to expand the patch area of an ACM2 spot weld model after mesh refinement. The programm needs a search radius as an input parameter. The programm connects the RBE3 elements with all shell corner nodes lying inside the given radius. The result of the expansion can be seen in figure (6.8).

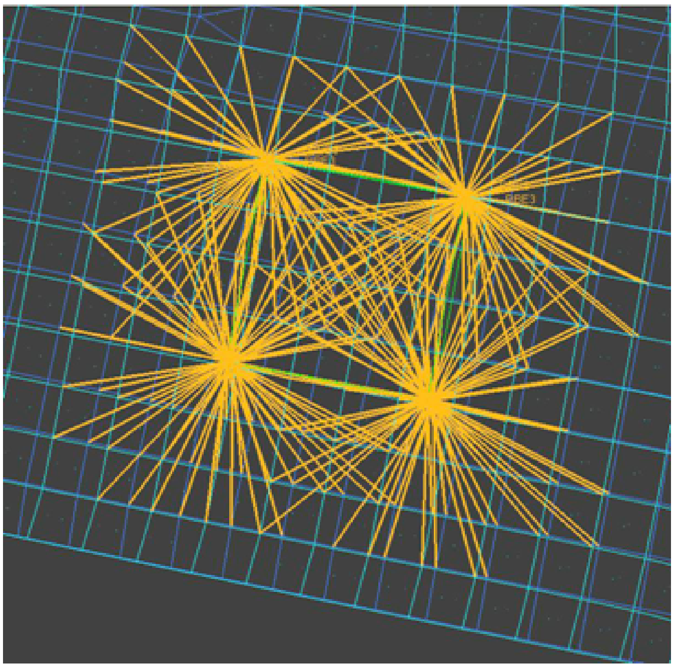

Figure 6.8: ACM2 spot weld after expansion of connection nodes

To compensate the loss in patch area which is responsible for the loss of bending stiffness it is necessary to know which search radius is the best one. Therefore different models with different patch areas have been calculated. Figure (6.9) one can see the result for different models where the search radius has been changed from 8 mm up to 15 mm. The thick solid curve represents the reference curve. This curve represents the mean change in frequency for the single panels when refine the panel mesh from 10 mm down to 5 mm.

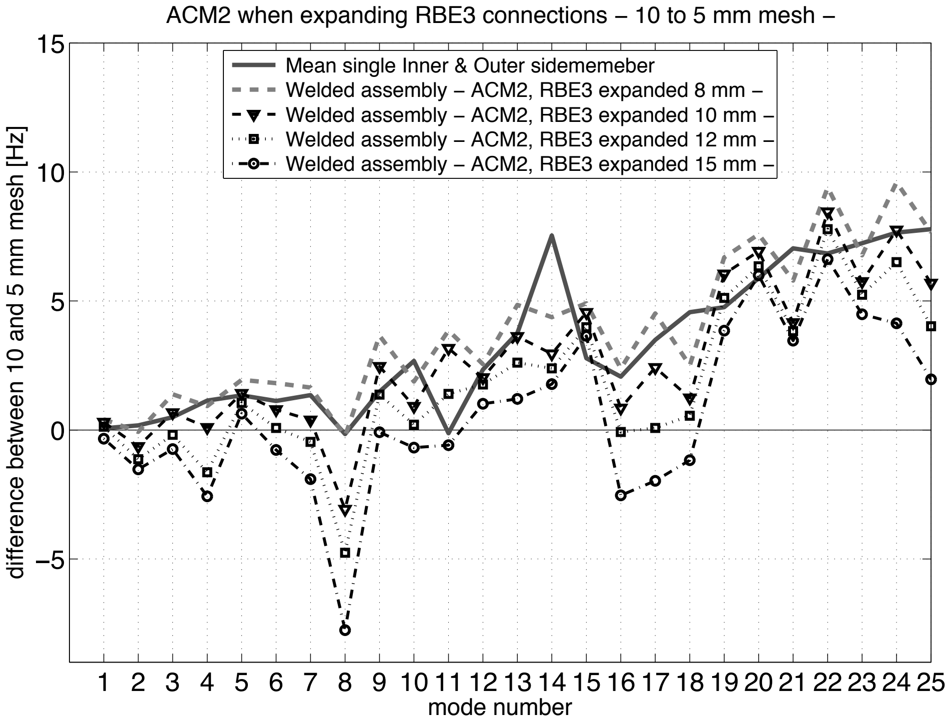

Figure 6.9: Mean change in frequency with different search radius via "RBE3 expansion" code for the first 25 mode numbers

One can see that a used search radius with 8 mm (dashed curve without markers) gives the smallest deflection to the reference curve. When increasing the patch area with an 8 mm search radius after mesh refinement from 10mm to 5mm, the ACM2 influence should nearly be eliminated. When now calculating the modified 5 mm and 2.5 mm model the results in resonance frequency should show nearly the same stepping pattern in resonance frequency like for the single sidemembers. There the smallest mesh density should result in the smallest deviation to measurement. This is caused by the better approximation of geometry should still remain in the same order like for the single panels. In figure (6.10) on can see the results for the first 8 mode numbers.
The results show that the "RBE3 expansion" increases the bending stiffness of the structure but the stiffening effect is very inconstant over all mode numbers. Especially on the first mode number the 2.5 mm model has now a larger bending stiffness like the origin 10 mm model. On the second mode number the 5 mm model is the stiffest one. Thus the expected stepping is totally lost.

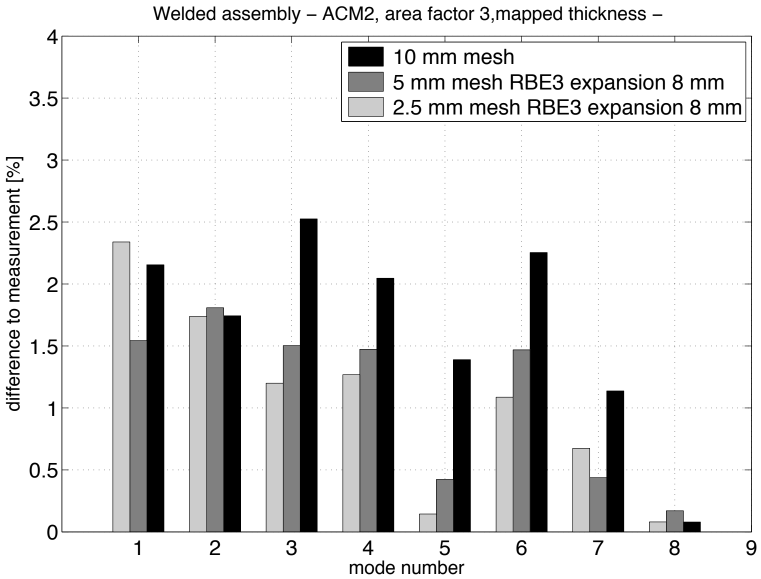

Figure 6.10: Deviation in % to measurement for refinement steps down to 2.5 mm mesh density

A detailed look on the RBE3 entries gives a first answer on what happened. Like Figure (6.6) shows, after applying the "RBE3 expansion" code on the FEM model the RBE3 element is not only connected with four shell corner nodes like the original ACM2 model. It rather connects all shell corner nodes lying inside the given search radius.

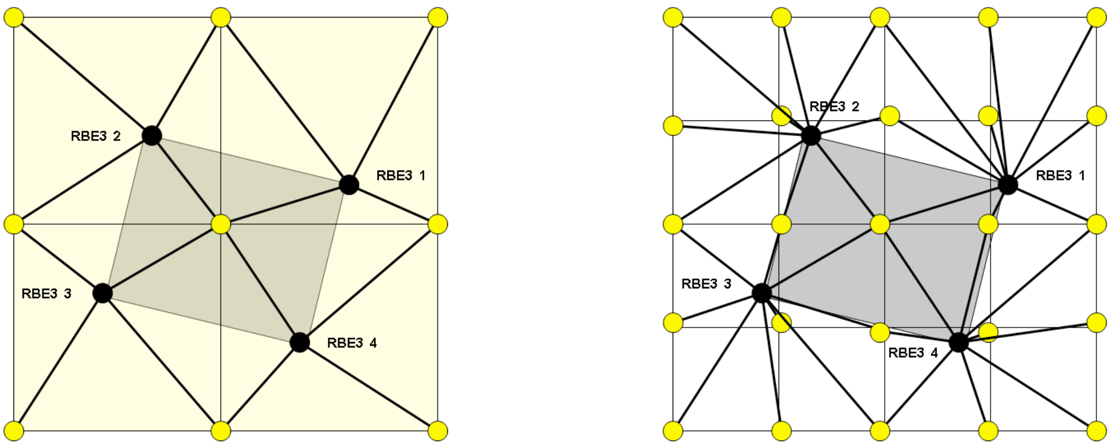

(a) origin ACM2 model

(b) reconnected with "RBE3 expansion" method

This connected nodes don't cover a typical shell element anymore. As a consequence the weighting factors of the RBE3 connection nodes depend not on the shape displacement functions anymore. Figure (6.11) shows an RBE3 entry of the modified geometry file. One can see the weighting (circles) factor is set to 1.0 for all connection nodes.

```
RBE3       43187            42757      123      1.      123    21449    21451+001127B
+001127B   27949    28010   37982    38755   39323    39324    41753
RBE3       43188            42758      123      1.      123    27986    27992+001127D
+001127D   27994    27998   28004    28010   38103    39323    39324    41753+001127E
+001127E   41754
```

Figure 6.11: RBE3 entry after application of expansion code

That means that if a force is applied to the RBE3 element, the resulting forces on the connected nodes will be distributed equally weighted depending on the amount of connection nodes. The weighting depending on the shape function of the underlying shell element is lost. As a consequence one can assume the stiffness near field around the spot weld not longer as a monopol with an equal stiffness distribution in all directions. Thus bending waves will be affected differentially depending on the angle of incidence. As a result the loss of stiffness due to mesh refinement will be compensated but not equally over the whole frequency range.

6.6 "RBE3 reconnection" on ACM2 model

Like the previous investigations have shown it is very important that the connection pattern from the original ACM2 model is kept constant when refining the mesh density. And also the amount of connected shell corner nodes should be the same like for the origin ACM2 model. The only way to ensure these conditions is to keep the connection vectors of the origin RBE3 connections and to reconnect these vectors after mesh refinement with the origin nodes of the FEM model again. Figure (6.12) illustrates the desired way.

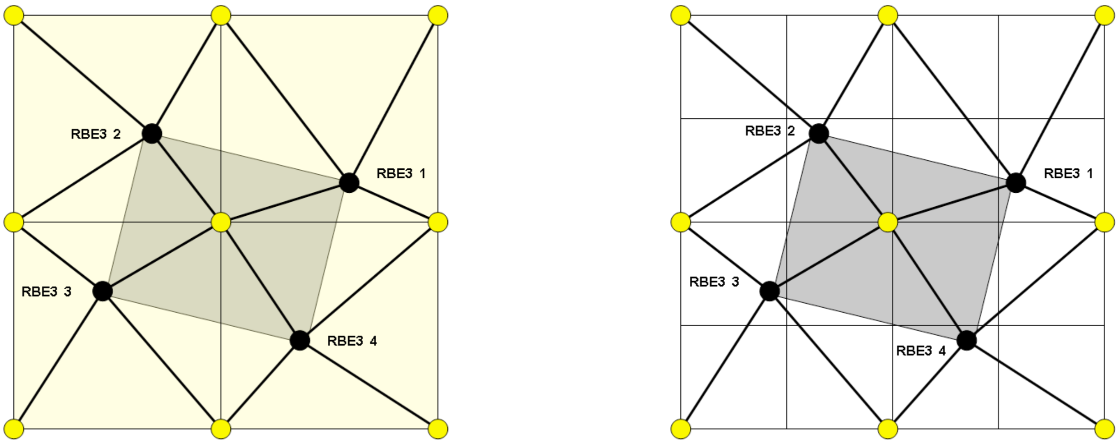

(a) origin ACM2 model

(b) reconnected after mesh refinement

Figure 6.12: The origin connection pattern of an ACM2 model in comparison to the modified ACM2 model with the "RBE3 reconnection" method

The main problem is of course that after mesh refinement the position of the origin nodes doesn't exist anymore. The reason therfore is when refining the mesh on the existing geometry the origin nodes will also be shifted. This happens because the finer mesh approximates the structer better like the old one. When copying the origin RBE3 connection vectors in the new created FEM model the vectors have to find the nearest lying nodes in some way. This problem could be fixed with the software *Hypermesh*. The four reconnected nodes now encircle a patch area corresponding to the origin one in the 10 mm mesh. The displacement of the RBE3 element depends now only on the weighted average of the displacements of these four surrounding nodes like before. In a similar way the weighting factors depends only on the shape displacement function describing the element encircled by the four connected nodes, regardless how many shell elements actually are lying inside this area. Figure (6.13) shows the results for a mesh refinement down to 2.5 mm.

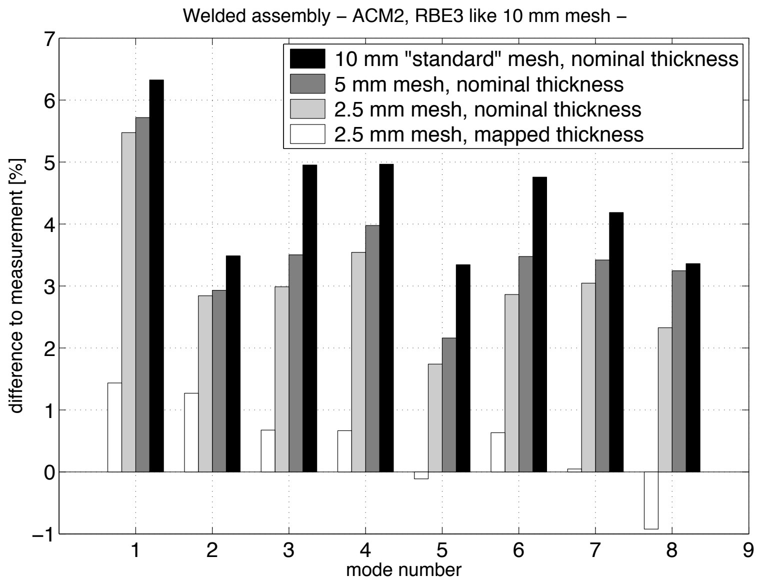

Figure 6.13: Deviation in [%] to measurement for models with nominal and mapped thickness

The figure (6.13) shows the deviation between the calculated natural frequencies and the measured ones in [%]. In comparison to the results from section (6.5) the finer the used meshes the smaller the deviation to measurement over all mode numbers. So the stepping due to mesh refinement is there again like observed at the single sidemembers. Also with nominal thickness the mean deviation to measured resonance frequencies in [%] is in the same order of magnitude like for the single sidemembers. This indicates that no additional stiffness has been introduced. The stepping pattern over all mode numbers shows also that the stiffness around the spot welds is now radiating equally in all directions. The figure (6.13) shows also the results for a 2.5 mm mesh with mapped thickness distribution. Here we can see that especially at mode number 5 and 8 the calculation results are below the measured ones. Like mentioned before the patch area of each ACM2 model still differs. This effect still remains from the beginning in the model and could be an explanation for the additional loss in stiffness at particular modes.

The results show that when keep the patch area of the origin spot weld model when refining the panel meshes the simulation results converge more on the measured results. The loss of bending stiffness due to the ACM2 model itself becomes insignificantly. This behaviour can also be observed in a FRF plot like presented in figure (6.14). There the 10 mm "standard" model with nominal thickness distribution shows a larger deviation compared with the measured curve. The implementation of the "RBE3 reconnected" ACM2 model, with a 2.5 mm mesh and mapped thickness leads to a quite good approximation of the measured mobility, even up to 400 Hz. Especially the eigenfrequencies of the "RBE3 reconnected" curve are not falling significantly below the measured ones. This shows that the discovered "RBE3 reconnection" method makes the ACM2 approach suitable for each mesh size smaller than 10 mm, which is a interesting result of the investiagtions in this work.

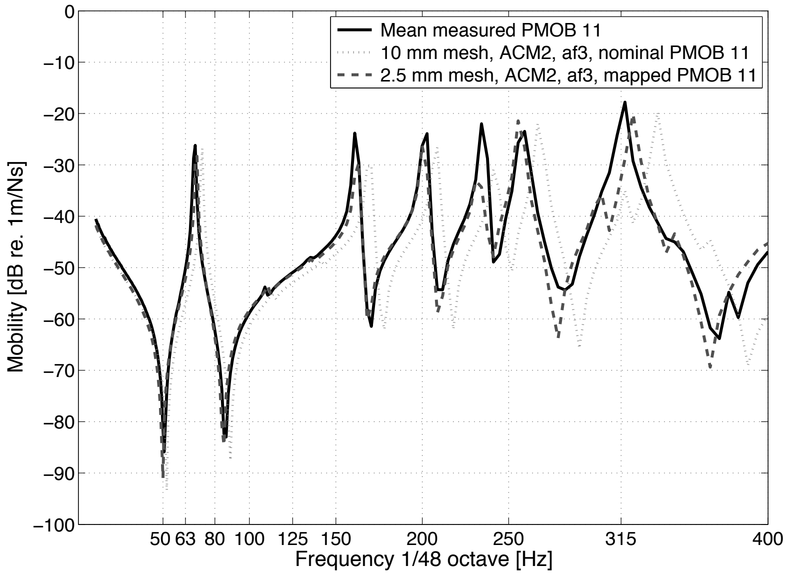

Figure 6.14: FRF comparison between a measured point mobility and the corresponding 10 and 2.5 mm model with the "RBE3 reconnected" ACM2 approach

7 Conclusion

In this Master's Thesis the influence of a mapped thickness distribution and refined panel meshes on a benchmark FEM model has been analysed. The benchmark structure was a complex three dimensional sidemember from a current Volvo car body. The investigations have been done for both the single panels and the welded structure.

The results show clearly that introducing a mapped thickness distribution leads to a significant improvement of the simulation results. For the single sidemembers and the welded assemblies the deviation between measured and calculated eigenfrequencies could be reduced of ca. 3% in a frequency range up to 300 Hz. So the deviation in eigefrequencies is less than 2% for the first ten modes with a mapped thickness. A additional advantage is that the improvement due to mapping works nearly unimformly for all modes and is a result of a better approximation of the local bending stiffness distribution.
Also the potential of the most common spot weld modelling techniques in NVH (ACM2 and CWELD) have been investigated with respect to the accuracy and robustness to refined panel meshes. The standard mesh size of 10 mm was refined down to 5, 2.5 and 1 mm. There the results show that the CWELD model is not applicable for panel meshes smaller than 5 mm because of its functional limitations. The investigations on the ACM2 model shows that when keeping the patch area like for the 10 mm standard mesh size no additional loss of bending stiffness is introduced by the spot weld model itself. The "RBE3 reconnection" method of the origin shell corner nodes makes the ACM2 model adaptable for all refined meshes. In general the efficiency of refining the mesh size is very much dependent on the frequency range of interest. For the sidemember panels the largest improvement could be achieved with the refining step from 10 down to 5 mm. There the FE-calculated eigenfrequencies up to 300 Hz could be improved in average of approximatly 0.5%. The other two refinements didn't change the first ten eigenfrequencies significantly. But it's clearly visible that with growing frequency the influence of mesh refinements is also increasing. So it really depends on the concrete situation which refinement step is reasonable.

For further application of the "RBE3 reconnected" ACM2 model it will be necessary to develop an "RBE3 reconnection" code which is applicable in the standard Preproccessor software available in industry. Here it should be also mentioned that in future there will be a demand to implement ACM2 models directly in FEM meshes smaller than 10 mm, without the use of existing connection vectors from previous models. For such goals the introduction of a search radius representing the average length of the RBE3 connection vectors of the 10 mm standard mesh size could be a solution.

References

[01] Palmonella, M.; Friswell, M.I.; Mottershead, J.E.; Lees, A.W.: *Guidlines for the implementation of the CWELD and ACM2 spot weld models in structural dynamics*, Finite Elements in Analysis and Design 41 (193-210), 2004

[02] Fang, J.; Hoff, C.; Holman, B.; Mueller, F.; Wallerstein, D.: *Weld modeling with MSC.Nastran*, Second MSC WorldWide Automotive User Conference, Dearborn,MI, USA, October 2000

[03] Heiserer, D.; Chargin, M.; Sielaff, J.: *High Performance, Process Oriented, Weld Spot Approach*, First MSC WorldWide Automotive User Conference, Munich, Germany, September 1999

[04] Jonscher, A.; Lewerenz, M.; Lührs, G.: *MSC.Nastran's new spot weld element in the CAE process*, Volkswagen A.G., Wolfsburg, Germany

[05] Xu, S.; Deng, X.: *An evaluation of simplified finite element models for spot-welded joints*, Finite Elements in Analysis and Design 40 (1175-1194), 2004

[06] Palmonella, M.; Friswell, M.I.; Mottershead, J.E.; Lees, A.W.: *Finite element models of spot welds in structural dynamics: review and updating*, Computers and Structures 83 (648-661), 2005

[07] Donders, S.; Brughmans, M.; Hermans, L.; Tzannetakis, N: *The effect of spot weld failure on dynamic vehicle performance*, LMS International, Leuven, Belgium

[08] Silva, J.M.M.; Batista, F.C.; Maia, N.M.M.: *Dynamic modelling of spot welded joints*, Twelfth International Congress on Sound and Vibration, Lisbon, 2005

[09] MSC.Nastran 2003: *Linear Static Analysis Users Guide*, MSC.Software Corporation, Santa Ana, CA 92707 USA

[10] MSC.Nastran 2005: *Quick Reference Guide*, MSC.Software Corporation, Santa Ana, CA 92707 USA

[11] Bretl, J.L.: *Connecting solid finite element models that have dissimilar meshes on the mating surfaces*, Structural Dynamics Research Corporation, Milford, Ohio; USA

[12] Cook, R.D.: *Finite Element modeling for stress analysis*, University of Wisconsin-Madison, John Wiley & Sons, Inc., 1995

[13] Ewins, D.J.: *Modal Testing theory, practice and application -Second Edition-*, Research Studies Press LTD., Baldock, Hertfordshire, England, 2000

[14] Chen, G.: *FE model validation for structural dynamics*, PhD Thesis, Dynamics Section, Department of Mechanical Engineering, London, South Kensington, April 2001

[15] Petyt, M.: *Introduction to finite element vibration analysis*, Cambridge University Press, Cambridge,1990

[16] Kropp, W.: *Technical Acoustic 1*, Department of Applied Acoustic, Chalmers University of Technology,2005

[17] Friswell, M.I.; Mottershead, J.E.; Lees, A.W.: *Finite element model updating in structural dynamics*, Kluwer Academic Publisher, Dodrecht, 1995

[18] Palmonella, M.: *Improving finite element models of spot weld s in structural dynamics*, PhD Thesis, University of Wales Swansea, 2003

[19] MSC.Nastran 2004: *Reference Manual*, MSC.Software Corporation, Santa Ana, CA 92707 USA

[20] MSC.Nastran Version 68: *Basic Dynamic Analysis User's Guide*, MSC.Software Corporation, Santa Ana, CA 92707 USA

A Single sidemember panels

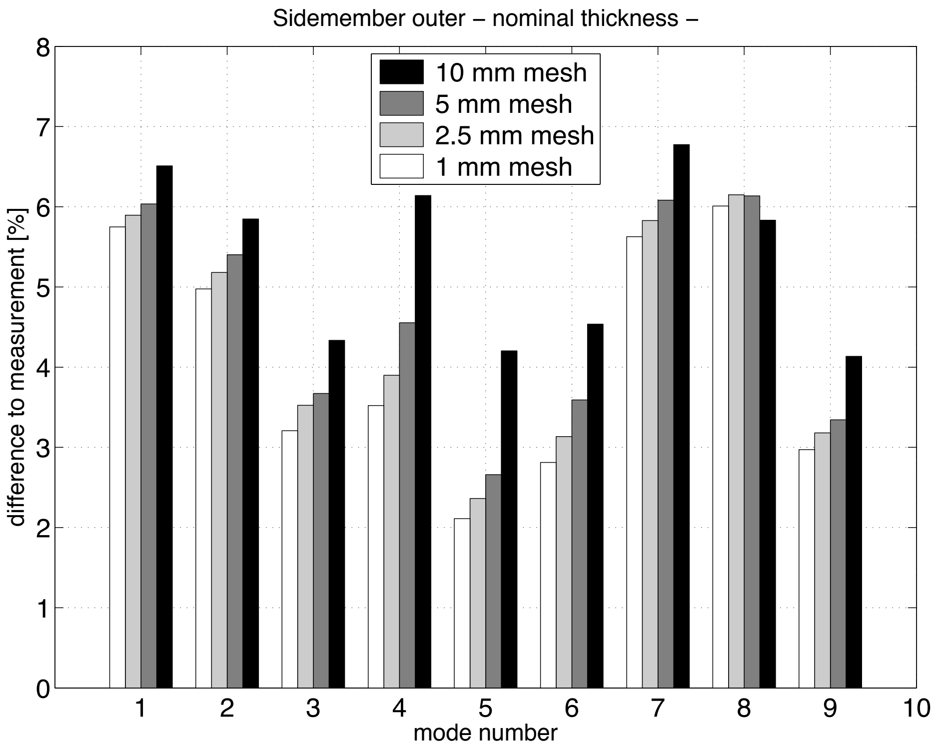

Figure A.1: Differences in eigenfrequencies for the first ten modes of the outer sidemember, due to mesh refinement

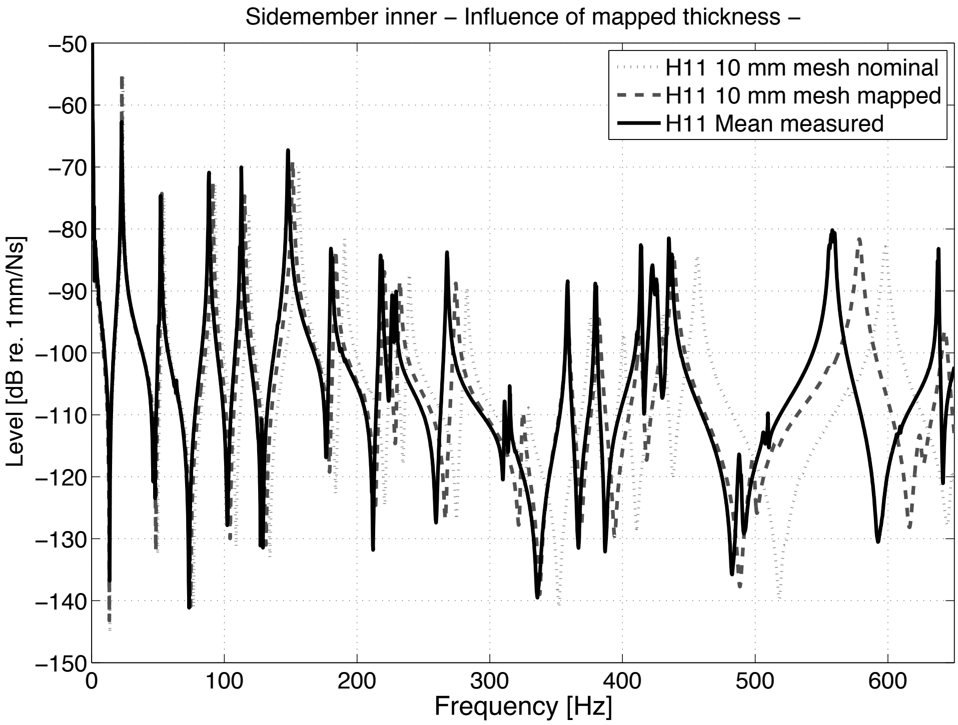

Figure A.2: FRF comparison to show the influence of mapping - extended frequency range